



Nanoscale

**Gas Hydrates in Confined Space of Nanoporous Materials:
New Frontier in Gas Storage Technology**

| | |
|-------------------------------|--|
| Journal: | <i>Nanoscale</i> |
| Manuscript ID | NR-REV-02-2021-000751.R1 |
| Article Type: | Review Article |
| Date Submitted by the Author: | 17-Mar-2021 |
| Complete List of Authors: | Both, Avinash Kumar; University of Nebraska-Lincoln, Department of Chemistry Gao, Yurui; University of Nebraska-Lincoln, Department of Chemistry Zeng, Xiao Cheng; University of Nebraska-Lincoln, Department of Chemistry Cheung, Chin Li; University of Nebraska-Lincoln, Department of Chemistry |
| | |

SCHOLARONE™
Manuscripts

ARTICLE

Gas Hydrates in Confined Space of Nanoporous Materials: New Frontier in Gas Storage Technology

Avinash Kumar Both,^a Yurui Gao,^a Xiao Cheng Zeng,^a and Chin Li Cheung^{*a}

Received 00th January 20xx,
Accepted 00th January 20xx

DOI: 10.1039/x0xx00000x

Gas hydrates (clathrate hydrates, clathrates, or hydrates) are crystalline inclusion compounds composed of water and gas molecules. Methane hydrates, the most well-known gas hydrates, are considered a menace in flow assurance. However, they have also been hailed as an alternative energy resource because of their high methane storage capacity. Since the formation of gas hydrates generally require extreme conditions, developing porous material hosts to synthesize gas hydrates with less-demanding constraints is a topic of great interest to the materials and energy science communities. Though reports of modeling and experimental analysis of bulk gas hydrates are plentiful in the literature, reliable phase data for gas hydrates within confined spaces of nanoporous media has been sporadic. This review examines recent studies of both experiments and theoretical modeling of gas hydrates within four categories of nanoporous material hosts that include porous carbons, metal-organic frameworks, graphene nanoslits, and carbon nanotubes. We identify challenges associated with these porous systems and discuss the prospects of gas hydrates in confined space for potential applications.

1. Introduction

1.1 Gas Hydrates: Overview and Crystal Structures

Gas hydrates (clathrate hydrates, clathrates, or hydrates) are exceptional non-stoichiometric encapsulating compounds capable of entrapping small guests such as gas molecules, ions, or radicals in cages made of hydrogen-bonded water molecules at specific temperatures and pressure.^{1, 2} Under these conditions, water freezes to construct a crystalline matrix of ice-like cages that host guest gas molecules (Fig. 1).³ With the first discovery of chlorine hydrate by Humphry Davy⁴ in 1810, the desire to understand water was accelerated and it expanded the water research to this new field of gas hydrates. The novel ice-like frameworks of water cages in gas hydrates are reinforced by hydrogen bonding and the van der Waals interactions among gas guests and water molecules.⁵⁻⁷ Gas hydrates occur naturally in large quantities all over the world.⁸ It is estimated that 6.4 trillion tons of methane are trapped within the methane hydrate deposits in the ocean floor.⁹ Conventionally, methane hydrates (or natural gas hydrates) have been seen as a menace that causes significant complications for the oil and natural gas industry in gas pipelines, during oil drilling processes, and in workover operations.^{10, 11} It was first discovered in 1934 that the reason for blockages in gas pipelines was due to the formation of methane clathrate hydrate plugs inside the gas pipelines instead of ice, which was initially perceived to be the reason behind the blockage.¹² The formation of methane hydrate inside the gas pipeline can weaken the structural integrity of the

gas pipelines and cause disruptions to the methane production process with high risk and low efficiency.¹³ Methane hydrates have also been identified as a primary cause of the deep-water flow assurance problem.^{11, 14} These natural gas hydrates, apart from being a menace, are now being explored as an eco-friendly and sustainable energy resource in the future because methane has important advantages as an energy resource in comparison to conventional fuels in terms of energy density and efficiency, cost of extraction and transportation, and environmental

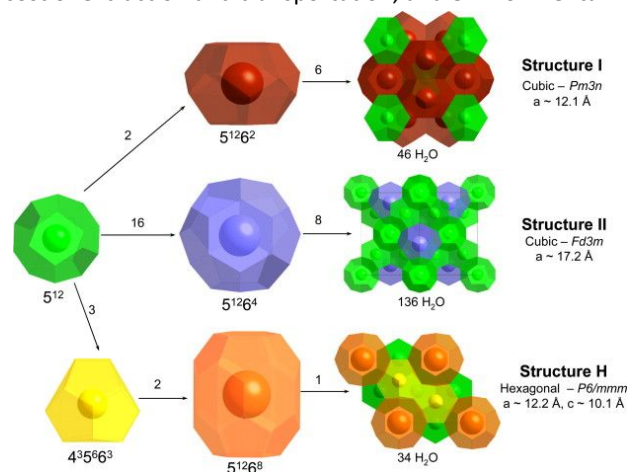


Fig. 1 Crystal structures (X^n) of structure I (SI), structure II (SII), and structure H (SH) of gas hydrates.^{8, 15} “X” denotes the number of sides of a polyhedral face, and “n” indicates the number of cage faces with X sides. Reproduced with permission from Ref.¹⁵. Copyright 2009, Elsevier Publishers.

impact.^{16, 17} Different categories of gas hydrates have been explored for their prospective applications in gas storage

^a Department of Chemistry, University of Nebraska-Lincoln, Lincoln, Nebraska 68588, U.S.A.

Table 1 Pore size in various cages of bulk gas hydrate structures.⁸

| Hydrate Crystal Structures | sI | | sII | | sH | | |
|----------------------------------|-----------------|--------------------------------|-----------------|--------------------------------|-----------------|--|--------------------------------|
| | Small | Large | Small | Large | Small | Medium | Large |
| Cavity | Small | Large | Small | Large | Small | Medium | Large |
| Description | 5 ¹² | 5 ¹² 6 ² | 5 ¹² | 5 ¹² 6 ⁴ | 5 ¹² | 4 ³ 5 ⁶ 6 ³ | 5 ¹² 6 ⁸ |
| Number of cavities per unit cell | 2 | 6 | 16 | 8 | 3 | 2 | 1 |
| Average cavity radius (Å) | 3.95 | 4.33 | 3.91 | 4.73 | 3.91 | 4.06 | 5.71 |
| Coordination number | 20 | 24 | 20 | 28 | 20 | 20 | 36 |
| Number of waters per unit cell | 46 | | 136 | | 34 | | |

media¹⁸, gas separation system^{17, 19-25}, energy storage media²⁶⁻³¹, energy transport³²⁻³⁵, cold energy storage^{36, 37}, carbon sequestration³⁸⁻⁴¹, and water desalination applications.⁴²⁻⁴⁴

One of the most distinguishable characteristics of a bulk gas hydrate is its ice-like cage structures that host guest gas molecules.⁴⁵ Conventionally, there are three conventional classes of bulk gas hydrate structures: structure I (sI) hydrate, structure II (sII) hydrate, and structure H (sH) hydrate⁴⁶ (Fig. 1 and Table 1). These different structures of water cages in gas hydrates are generally labeled as Xⁿ, where “X” denotes the total number of sides of a polyhedral face and “n” denotes the number of cage faces having X sides. Different gas hydrate structures have distinct numbers of cages and cage volumes per unit cell. For example, an sI hydrate has two distinct cage-types, a small pentagonal dodecahedral cage represented by 5¹² (consisting of 12 pentagonal faces on the cage) and a relatively large tetrakaidecahedral cage represented by 5¹²6² (12 pentagonal and 2 hexagonal faces on the cage). However, an sII hydrate is composed of small 5¹² cages and large hexacaidecahedral cages denoted by 5¹²6⁴ (12 pentagonal and 4 hexagonal faces on the cage). In contrast, an sH hydrate consists of small 5¹² cages, medium-sized 4³5⁶6³ cages (3 square, 6 pentagonal, and 3 hexagonal faces on the cage), and large icosahedral cages, denoted by 5¹²6⁸ (consisting of 12 pentagonal and 8 hexagonal faces on the cage).²

The type of crystal structure that constitutes the unit cell of a gas hydrate is highly dependent on the size and the geometry of the guest gas molecule. Small gas molecules including methane and ethane tend to form the sI hydrate structure, but bigger gas molecules such as C₃H₈ tend to form the sII hydrate structure.^{5, 47-49} Guest-free hydrates are generally thermodynamically unstable because the ice-like porous structures have to be partially stabilized by the gas molecules entrapped in the cages. Nonetheless, Falenty and co-workers successfully synthesized the guest-free sII hydrate by leaching the guest neon atoms from the sII structure of neon hydrate.⁵⁰ Computer simulations have also been widely applied to predict bulk guest-free hydrates⁵¹ and they are usually specified using the nomenclature of microporous material zeolites such as RHO⁵², FAU⁵³, and EMT.⁵⁴ However, these computer-simulated guest-free hydrates are predicted to be thermodynamically stable at strongly negative pressures.

1.2 Gas Hydrates in Nature

Natural gas hydrates are primarily found in the oceanic and permafrost regions.⁵⁵⁻⁵⁷ At present, the explored methane

hydrate reservoirs on the ocean floor are mainly distributed in Japan, India, Gulf of Mexico, Bering Strait, South China Sea, Korea, Trinidad, and Tobago. Natural gas hydrates in the permafrost are primarily distributed in Alaska, Mackenzie Delta, Qinghai-Tibet plateau, and Siberia.^{5, 8} The source of methane in these naturally occurring gas hydrates is largely through methanogenesis, in which the methanogens (bacteria) break down and reduce organic matter over time to evolve methane.⁵⁸ Production methods to extract methane from these natural gas clathrate hydrates are currently being developed as a lucrative alternate energy resource.²⁹ Natural gas hydrates in the permafrost region exist not only in the clay layer but also in the pores of the sandy sediment (Fig. 2).^{55, 59} It is known that the demanding conditions for storing methane in hydrates at low temperatures (liquefied natural gas at 111 K) or enormously high-pressure requirements (compressed natural gas at 25 MPa) are highly undesirable and expensive.^{5, 60}



Fig. 2 Schematic showing methane hydrates in hydrate-bearing sediments found in nature.⁶¹ Reproduced with permission from Ref.⁶¹. Copyright 2020, Elsevier Publishers.

Besides being a potential energy resource, gas hydrates have been studied for developing hydrate-based seawater desalination technology since the 1940s.^{3, 62, 63} In this hydrate-based desalination process, seawater is pressurized with co-former agents that can induce the formation of hydrates. Consequently, water molecules in seawater encapsulate the hydrate forming agents and form the hydrate crystals, thereby excluding salt and other impurities from being incorporated

within the hydrate structure.⁶⁴ Afterward, the hydrate crystals are then mechanically removed and decomposed into potable water and hydrate forming agents that can be recycled to resume the desalination process (Fig. 3).⁶²

Significant research efforts have been made globally to harness the hydrate-based desalination technology due to its potential eco-friendliness and economic feasibility.⁶⁵ Currently, to accelerate the hydrate growth kinetics and alleviate the high-pressure requirement, an array of hydrate forming agents such as propane⁶⁶, cyclopentane⁶⁷, carbon dioxide⁴², refrigerant gases (HFC, HCFC, and CFC),^{68, 69} and sulfur hexafluoride⁷⁰ have been studied as possible candidates for the hydrate-based desalination technology.⁷¹⁻⁷⁵ Porous materials have been documented as hydrate carriers because they can promote the nucleation of gas hydrates due to their high surface area.⁷⁶⁻⁷⁸ The specific hydrophobicity of these materials can further enhance the contact surface between immiscible water and hydrocarbons for forming hydrocarbon clathrate hydrates.⁷⁹ Hence, porous materials could be useful in ameliorating the extreme pressure and temperature required for improving the hydrate-based desalination process.

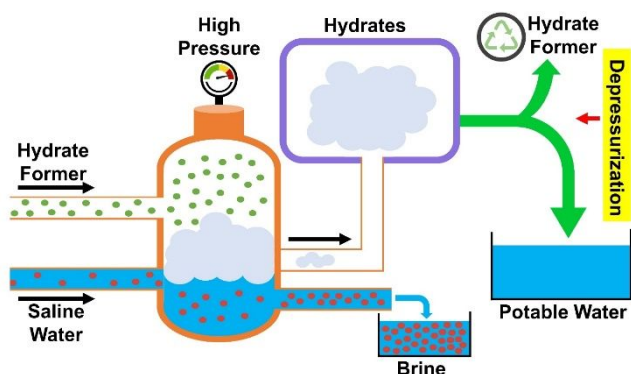


Fig. 3 Schematic illustration depicting the hydrate-based desalination process. In this process, saline water is pressurized with a hydrate forming agent to form hydrates. The hydrate crystals can then be isolated from the brine and depressurized to give potable water and hydrate former which can be recycled.

Understanding the formation of gas clathrate hydrates in small pores is of fundamental importance because natural gas clathrate hydrates in the seabed are dispersed in the pores of deep-sea sediments typically comprising of 1-nm thick layers.⁴⁵ Additionally, the thermodynamic behavior of gas clathrate hydrates confined within these layers is expected to be significantly different from those of bulk gas clathrate hydrates.⁸⁰ The characteristics of highly confined water stem from an interplay between the hydrogen-bonding interactions and spatial homogeneity under the confinements in the nanosized pores.^{81, 82}

1.3 Gas Hydrates in Porous Media

The research on exploring confinement effects to induce the growth of gas hydrates within porous materials at moderate conditions is becoming increasingly popular in the field of gas hydrates.⁸³ Gas hydrate research has been expanded to a broad

range of porous materials in the past few decades.⁸⁴ The unique behavior of gas hydrates within porous materials including silica gels (SGs)⁸⁵⁻⁸⁸, porous glasses (PGs)⁸⁹⁻⁹², graphene oxide (GO)⁹³, sand⁹⁴⁻⁹⁶, and clay^{97, 98} have been reported. Preliminary studies of porous materials focused on exploring the behavior of gas hydrates in the confined environments found in porous geosediments.⁹⁹⁻¹⁰¹ Currently, the newly found properties of confined gas hydrates and increasing scientific curiosity to understand their formation kinetics at the nanoscale have driven this new pioneering field to embrace new applications such as gas storage media and gas separation systems.¹⁰² It has been illustrated that the geometric constraints in porous media affect many characteristics of gas hydrates including hydrate cage occupancy, hydrate growth kinetics, and thermodynamic phase behavior.^{85, 103} The distinctive phase behavior of water under nanoscale confinement stemmed from the hydrogen-bonding interactions and spatial inhomogeneity which significantly impacts the kinetics of crystallization.¹⁰⁴⁻¹⁰⁶ Besides the discussed applications in energy storage and desalination, other examples include selecting boundary lubrication condition in nanofluidic devices^{107, 108}, frost heaving phenomenon in soil^{109, 110}, syntheses and designs of antifreeze proteins to inhibit ice growth^{111, 112}, rapid cooling of biological suspensions under high pressure^{113, 114}, extractions of natural gas from shale rock^{115, 116}, and understanding the gas trapping phenomenon within interstellar ices.¹¹⁷⁻¹¹⁹ In this review, we survey recent theoretical models and experimental findings for understanding the growth of gas hydrates within confined spaces of nanoporous materials. We focus on examining recent findings in four categories of nanoporous materials that include porous carbons, metal-organic frameworks, graphene nanoslits and their applications in energy gas storage, carbon sequestration and seawater desalination (Fig. 4). Lastly, we will discuss the prospects and challenges in the field of gas hydrates formed within confined spaces.

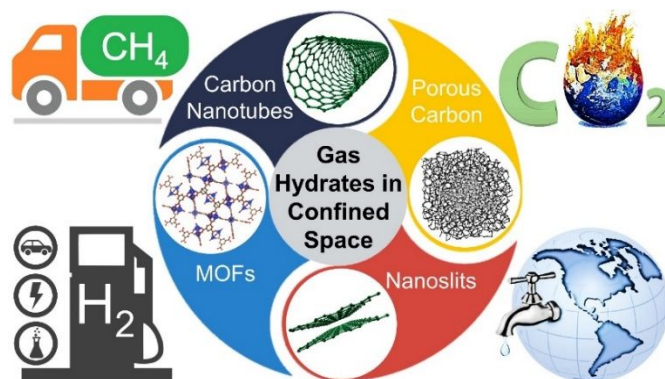


Fig. 4 Schematic illustration depicting four categories of nanoporous materials for growing gas hydrates in confined spaces and their applications in energy gas storage, carbon sequestration, and water desalination.

2. Gas Hydrates in Porous Carbon

Porous carbon is a highly porous material that has a complex structure consisting predominantly of carbon atoms.¹²⁰ Porous carbon is a member of a family of carbons ranging from carbon

blacks, carbon fibers, and carbon composites. They are all derived from common sources but with different carbonization and manufacturing processes.¹²⁰ Porous carbon is a unique material because of the way it is filled with "pores" that significantly enhance its surface area. The porosity (pore size) of these materials can be enhanced by two processes: physical activation and chemical activation. During the physical activation, gases such as H₂, H₂O, and O₂ enter the pores and gasify the surface atoms of the pores, thereby removing carbon atoms as CO₂, CO, H₂, and CH₄.¹²⁰ For chemical activation, modifications are achieved in the carbonization process by adding chemical additives to the solid carbon precursor such as H₃PO₄, ZnCl₂, KOH, and K₂CO₃.¹²⁰ ZnCl₂ and H₃PO₄ produce a dehydrating effect on the carbon precursor, resulting in a reduction in the particle size. ZnCl₂ drives the creation of small and uniform size micropores, whereas H₃PO₄ leads to a heterogeneous microporosity. In the case of KOH, the carbon precursor is oxidized to CO or CO₂, creating some porosity and K₂CO₃. In this process, KOH is reduced to potassium which is intercalated between the graphene layers of the carbon particles to generate micropores.

Understanding the relationship between porosity and surface functionality is essential for enhancing these porous materials' performance in different applications. Based on porosity, activated porous carbons are divided into three broad categories: microporous (< 2 nm), mesoporous (2 -50 nm), and macroporous (>50 nm) carbons.¹²⁰ Activated porous carbons possess big internal pore volumes that facilitate them to trap water and gas molecules.¹²¹ This outstanding ability to adsorb water molecules to attain good contact with gas molecules has been widely explored by researchers to investigate gas hydrate formation and phase behavior within different activated porous carbons.¹²²⁻¹²⁴

2.1 CH₄ Hydrates in porous Carbon

2.1.1. Effect of Pore Size

The formation of gas hydrates in different sizes of cavities in porous materials has been directly correlated with natural gas

hydrates found in sediments deep under the sea.¹⁰⁰ Understanding this phenomenon is advantageous for applications of porous materials as physisorption media and nanoreactors for growing artificial methane hydrates.¹⁰¹ Water molecules enclosed within pores of activated carbons were reported to enhance the adsorption of methane and the resulting combination tends to form methane hydrates under the pressure slightly higher than 3.5 MPa at 275 K.¹²⁶ One of the ground-breaking findings of the formation of methane hydrate within carbon materials goes back to 1998, in which Miyawaki *et al.* assessed methane adsorption at sub-par pressure (up to 0.03 MPa) in water-saturated porous carbons at 303 K.¹²⁷ Even with the limited pore volume in these porous carbons (with pore size under 1.1 nm) and the minimal pressure employed, a credible model of methane nanohydrates was proposed based on the experimental findings and the simulation of methane adsorption with a gas-to-water ratio of 1:2. This study illustrated the correlation of the gas hydrate growth process with the extent of fractional loading of the pores with pre-adsorbed water.

Pore volume also plays a vital role in the formation of gas hydrate within confined nanopores. Borchardt *et al.*¹²⁵ evaluated an array of model porous carbons (micro-, meso-, and macroporous) as shown in Fig. 5(a)-(d). They found that the pore volumes of these materials played major roles not only in calculating the net methane adsorption capability in saturated environments but also in determining the hydrate-to-water ratio percentage. Therefore, the integration of porous carbon nanostructures had a boosting impact on the formation of methane hydrate. Upon a closer examination of the methane isotherms, they revealed that all test materials in this study displayed critical blocking effects caused by water at the low-pressure range (below 2 MPa) (Fig. 5(e)). Nevertheless, the adsorbed methane quantity improved significantly in the pressure range of 2–4 MPa hinting towards the formation of methane hydrate. The adsorption capacity of methane within the micropores (C_{micro}, the pore size of 0.8 nm) was restricted to 180 mg/g due to spatial restraints. Similar results were

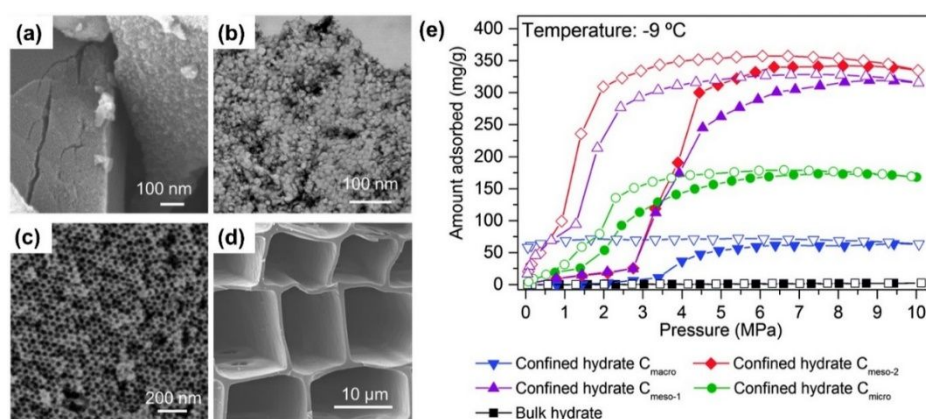


Fig. 5 SEM and STEM images of the four model carbons: (a) C_{micro} (0.8 nm), (b) C_{meso-1} (10 nm), (c) C_{meso-2} (25 nm), and (d) C_{macro} (10,000 nm). (e) High-pressure isotherms studying methane adsorption/desorption at 264 K in different carbons.¹²⁵ Reproduced with permission from Ref.¹²⁵. Copyright 2016, PCCP Owner Societies.

observed from pinewood-derived macro-porous carbons (C_{macro} , the pore size of 10,000 nm). However, in comparison to the dry carbons, mesoporous carbons exhibited an increase in the methane adsorption capacity of 120% and 173% for the 10 nm and 25 nm samples, respectively.

2.1.2 Effect of Water Content

An accelerating impact of the fractional loading in the quantity of methane trapped by water-saturated porous carbons (mesoporous and microporous) was observed by Celzard *et al.*¹²⁸ as well as Casco *et al.*¹²⁶ albeit under different conditions (275 K and up to 8–10 MPa). Generally, high-pressure isotherms of methane within the pores of these activated wet porous carbons are categorized into three major ranges of pressure: (1) pressure less than 4–5 MPa, results in less adsorption capacity in comparison to the dry porous carbons, (2) pressure range of 5–8 MPa at which an ensuing increase in the adsorption capacity credited to the formation of methane hydrate in large pores, and (3) pressure above 8 MPa denoting the formation of methane hydrate within the smaller pores (mesopores or micropores). A higher level of water saturation was found to be essential to bridge the adsorption capability of the dry porous carbons. The highest adsorption at 10 MPa was 50 wt.% for the water-saturated sample $R_w = 1.8$, which was higher than the dry porous carbons (24 wt.%), where $R_w = \text{weight of water/weight of carbon}$ (Fig. 6).¹²⁶ Reaching the point of oversaturation ($R_w = 4.1$) remarkably enhanced the methane storage capacity to 63 wt.%, through the addition of a step in the methane adsorption isotherm at 3.5 MPa. This was due to the growth of methane hydrate within the macropores. The gas hydrate growth within porous carbons was dependent on a sizable hysteresis loop resulting from the metastability of the gas hydrate growth process. At this stage, these gas hydrate crystals within confined nanospace were formed within 60 minutes. Thus, owing to the enhanced gas-liquid interphase, the presence of activated porous carbons accelerated the gas hydrate formation kinetics in a timescale comparable to that of the bulk phase.

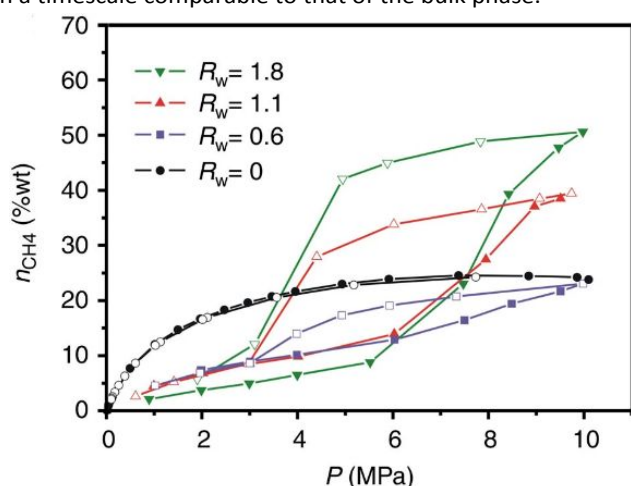


Fig. 6 High-pressure CH_4 isotherm studying adsorption/desorption of CH_4 on activated carbons under distinct water saturation ratios ($R_w = \text{weight of water/weight of carbon}$).¹²⁶ Reproduced by permission from Ref.¹²⁶. Copyright 2015, Springer Nature Publishing Group.

The growth kinetics of methane hydrate in water-saturated porous carbons was demonstrated by Yan *et al.* to increase upon a decrease in the formation temperature or an increase in the methane pressure.¹²⁹ This study suggested that to achieve the maximum formation of methane hydrate, the water-to-carbon weight ratio had to be optimized. Conditions by-passing that optimal ratio would plummet the amount of methane in the porous carbons due to the accumulation of bulk water above the water-filled carbon bed.

2.1.3 Effect of Particle Size

The particle size effect of activated porous carbons on the growth of methane hydrate has been investigated by Siangsai *et al.*¹³⁰ For activated porous carbons with large particle sizes (841–1680 μm), the high-pressure gas adsorption experiments (8 MPa and 276 K) resulted in a gas hydrate yield of 96%. This was attributed to the bigger interstitial pore gaps amongst the activated porous carbon particles. Activated porous carbon particles with small sizes (250–420 μm) also exhibited enhanced methane hydrate formation kinetics because their surface provided greater contact areas that allowed water and methane molecules to diffuse more efficiently. *In situ* thermal studies revealed two separate growth stages. The first stage was postulated to originate from the formation of imminent gas hydrate films within the interstitial space present at the gas-water interphase. The second stage was credited to the growth of gas hydrate within the core of the interparticle spacings through gaps and cracks created in the peripheral gas hydrate films.

Babu *et al.*¹³¹ reported the growth of methane hydrate in silica sand and activated porous carbons. They proposed that the nucleation of gas hydrate first began on the surface of carbon particles, whereas for silica, the gas hydrate crystals were formed within the interstitial gaps between the pores. Additionally, for activated porous carbons of larger particle sizes, the occurrence of a transient gas hydrate crystal within the hydrate stability region was observed. Jung *et al.*¹³² reported similar observations for methane hydrates formed within capillary pores, further indicating the intricacy of the nucleation mechanism and the growth process of gas hydrates within the confined environment.

2.2 Hydrate Growth Models in Porous Carbons

It has been well-established in the literature that all carbon surfaces can act as nucleation sites for gas hydrates because they enhance the water-gas interphase to facilitate the formation kinetics in comparison to the bulk gas hydrate phase¹³³. In the light of the kinetic growth model reported by Skovborg *et al.*¹³⁴, assuming that the diffusion of the guest gas molecules from the bulk gas phase to the bulk water is the rate-determining step, Yan *et al.* claimed that the surfaces of carbons play the key role in the nucleation of methane hydrates as opposed to the water/gas interface commonly credited for bulk hydrate growth.^{129, 135}

A recurring open question among the scientific community of hydrates centers on understanding the complex nucleation mechanism and the growth process of methane hydrates in the presence of porous carbons. Since the size of a thermodynamically stable gas hydrate nucleus is approximately 8–11 nm¹³⁶, the growth mechanism for understanding the formation of gas hydrates within macropores cannot be applied to micropores which have limited pore space for gas hydrate growth. Also, various water adsorption mechanisms are expected when compared to the case of larger pores. Nevertheless, there are several proposed mechanisms for micropores. According to one proposed growth mechanism, pure water first forms films on the surface of the cavities of the porous carbons, followed by the formation process of gas hydrate at the interface between water and the surface of the porous carbons (Fig. 7). This water film provides a larger and more effective contact area amongst the methane and water molecules to initiate the methane hydrate growth.

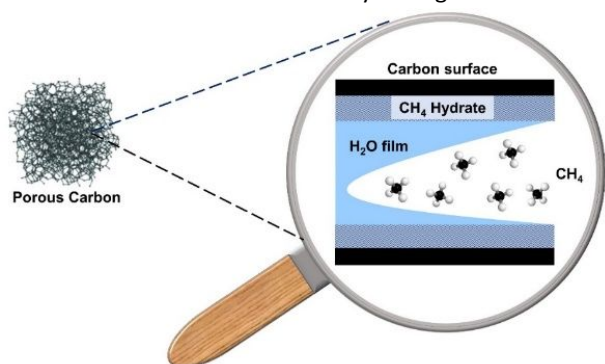


Fig. 7 A physical model for the formation of methane hydrate in activated porous carbons.¹²⁹ Reproduced with permission from Ref.¹³⁷. Copyright 2013, Hindawi Publishing Corporation.

One of the daunting challenges in this field is to resolve the crystal structure and morphology of the confined gas hydrates. After all, owing to the lack of experimental proof regarding the nature and structure of this potential gas hydrate formed under this spatial constraint, the nucleation mechanism and growth process in micropores is yet to be explored. The absence of experimental evidence lies in the limited crystal size of these confined gas hydrates in micropores being too small to be characterized using standard spectroscopic methods, although the crystal structure of the methane hydrate crystals formed in the confined environment of larger cavities has been reported using synchrotron X-ray diffraction.^{125, 126} These experimental studies have demonstrated that gas hydrate crystals formed within porous carbons with different pore sizes (mesoporous) reveal an *sl* gas hydrate crystal structure with an average crystal size of 10–50 nm. These meticulously constructed activated porous carbons can be used as gas hydrate growth media to synthesize artificial methane hydrates under moderate pressure and temperature environment (3.5 MPa and 275 K) with quicker hydrate growth kinetics (within minutes) than those in nature, fully reversible methodology, and a minimal stoichiometry that simulates the growth of natural gas hydrates.¹²⁶ However, activated porous carbons display

imperative challenges associated with the dearth of structural versatility in terms of composition and surface chemistry functionality.^{120, 138, 139}

3. Gas Hydrates in Metal-Organic Frameworks

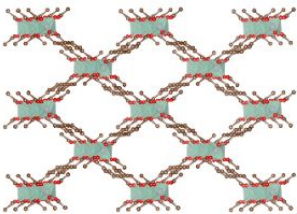
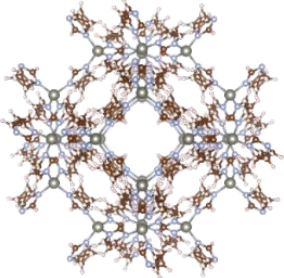
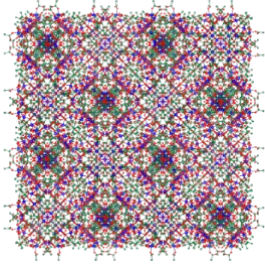
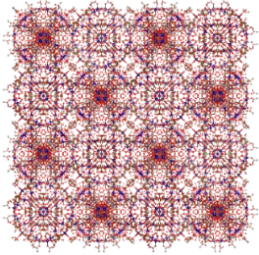
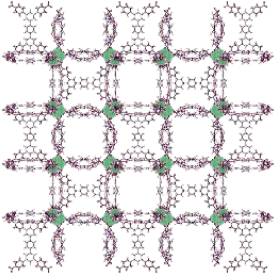
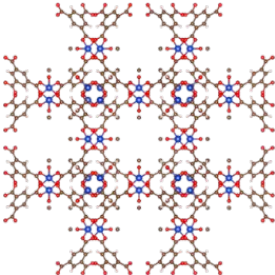
Metal-organic frameworks (MOFs), also known as porous coordination polymers (PCPs), are porous materials consisting of metal-ion networks linked by multifunctional organic molecules.¹⁴⁰ These linkages are formed through robust chemical bonds between the organic linkers and the metal-containing clusters.¹⁴¹ Through modifying the types of metal ions and organic linkers, a large assortment of different porous structures can be designed and synthesized with varied pore traits including size, shape, and density of the pores.¹⁴² According to the International Union of Pure and Applied Chemistry (IUPAC), one criterion that MOFs needs to satisfy is to contain cavities (voids) with no actual size limit for the porosity.¹⁴³ Hence, MOFs can be divided into three broad categories based on porosity: microporous (< 2 nm), mesoporous (2 - 50 nm), and macroporous (> 50 nm).¹⁴⁴ While different types of MOFs have been thoroughly explored for their applications as gas storage devices¹⁴⁵ and gas separation systems¹⁴⁶, researchers only started to realize the effect of water on enhancing the gas storage capacity and gas separation efficiency of MOFs in the past decade (Table 2).¹⁴⁷⁻¹⁵¹ This is because most MOFs developed at the beginning of this material research field had water-sensitive metal-organic linkages and thus were unstable in the presence of water.¹⁵²

3.1 CH₄ Hydrates in MOFs

Gas hydrates have been reported to form within the pores of MOFs and enhance their gas storage capacity. Recently, the formation of methane hydrate inside MOF MIL-53 was reported (Table 2).¹⁵³ MIL-53 was chosen in this study because it is thermodynamically stable in water and commercially available. MIL-53 consists of interconnected chains formed by aluminum hydroxide and benzene-1,4-dicarboxylates. This sequential linking of metal ions with organic molecules gives rise to a highly porous structure.¹⁵⁴ MIL-53 has two types of pores. The first type is the micropore of size around 0.6 nm (pore volume: 0.18 cm³ g⁻¹) and the second type is the meso/macropore of pore size more than 10 nm (pore volume: 0.49 cm³ g⁻¹). The nucleation of methane hydrate crystals was observed solely in the interparticle space (meso/macropores) instead of the inner micropores (Fig. 8(a)). This was attributed to the small size of the micropores (~0.6 nm) in comparison to the size of the *sl* unit cell for methane hydrate (~1.2 nm).

The formation of gas hydrates in MIL-53 was characterized by synchrotron high-resolution X-ray powder diffraction (HRPD) because the high-intensity synchrotron X-ray provides greater penetration depth and diffraction peak intensity. In this study, the water-saturated MIL-53 samples were pressurized with CH₄ (10 MPa) and CO₂ (4 MPa) at room temperature and also at 243 K. The corresponding HRPD data showed diffractions peaks corresponding to the diffractions from planes of *sl* gas hydrate. Additionally, P-T trace curves were measured to evaluate the phase transformation of the hydrates in MIL-53 (Fig. 8).

Table 2 Table showing the crystal structures of different metal-organic frameworks (MOFs) reported for hosting the growth of gas hydrates.

| MOF | Structure | Guest Gas | Ref. |
|--------------|---|-----------------------------------|------|
| MIL-53 |  | CO ₂ , CH ₄ | 153 |
| ZIF-8 |  | CH ₄ | 155 |
| MIL-100 (Fe) |  | CH ₄ | 156 |
| MIL-101 |  | CH ₄ | 157 |
| Cr-soc-MOF-1 |  | CH ₄ | 158 |
| HKUST-1 |  | CO ₂ | 147 |

The sharp drop in pressure in the cooling curve of the P–T traces (blue arrow) in both cases was indicative of the formation of the corresponding gas hydrates. The first gas hydrate phase observed at higher pressure and temperature was very similar to that of the bulk phase of gas hydrate, whereas the other gas hydrate phase was somewhat of a confined hydrate phase as a result of the limited dimensions of the pore. The growth of the bulk hydrate was only observed in the macropores (> 300 nm). Note that the amount of bulk phase of both gas hydrates in MIL-53 was insignificant in comparison to the confined phase of gas hydrate. In the case of CO₂, cooling and heating curves turned out to be different due to a pressure drop but no such pressure difference was seen in the case of CH₄. Interestingly, with 33 wt. % of water-saturation in MIL-53, no bulk phase of the gas hydrate was observed due to insufficient water. Inhibited phase behavior was exhibited by the confined hydrate phases of both CH₄ and CO₂ hydrates within MIL-53. This was because both the surface properties and the pore size influence the phase behavior of gas hydrates formed within a confined environment.

Zeolitic imidazolate frameworks (ZIFs) are another subclass of MOFs which are water-and-acid stable (Table 2). ZIFs have been reported to nucleate gas clathrate hydrates within their lattice structures for gas storage applications.^{159, 160} Mu *et al.* reported an increase of 45% in the gas storage capacity of ZIF-8 due to methane hydrate formation.¹⁵⁵ In this study, methane hydrates formed within ZIF-8 pores (pore volume: 0.61339 cm³ g⁻¹) at 269.15 K and 274.15 K. The phase behavior of methane hydrate was studied above and below 273 K (freezing point of water). Additionally, the effect of water content in ZIF-8 pores on the storage capacity of methane hydrate was studied at four different water content percentages (16.34%, 27.71%, 30.64%, and 35.13% (by mass)). The growth of CH₄ hydrate in ZIF-8 was observed only within the interparticle space between pores because water cannot access the hydrophobic inner pores.

The results showed an improvement in the methane storage capacity of ZIF-8 clusters along with ZIF-8 particle beds. For maximizing the methane storage capacity of the ZIF-8 particle bed (S_v), there was an optimal water content (~30%) required. There are two reasons behind this, firstly, the strong hydrogen bonding among water molecules makes the ZIF-8 particles more

attractive to each other. Secondly, the water molecules may have increased the pore volume of MOFs.¹⁶¹ The first effect decreased the volume of the water-filled ZIF-8 bed (V_b) whereas the second effect increases the V_b with increasing water content. The methane storage capacity of a water-filled ZIF-8 framework with a net water content of 35.13% was 56% (by mass) more than that of the dry ZIF-8 sample at 269.15 K and 2.85 MPa. The methane storage capacity of a water-filled ZIF-8 particle bed with a water content of 30.6% was 150 v/v at 6.5 MPa. The ZIF-8 framework remained stable during the water saturation of pores and the methane hydrate formation processes. No changes in the morphology after dissociation of methane hydrate in ZIF-8 were observed, demonstrating that it can be used repeatedly for methane hydrate formation.

The effect of porosity and surface chemistry of MOFs on the nucleation of the methane hydrate have been reported using the hydrophilic MIL-100 (Fe) MOF and the hydrophobic ZIF-8 MOF (Table 2).¹⁵⁶ MIL-100 (Fe) is a hydrophilic MOF that has large mesopores (2.4–2.9 nm) and micropores (0.55 nm and 0.86 nm).¹⁶² ZIF-8 has a hydrophobic external surface and internal pore cavities of about 1.2 nm.¹⁶³ The methane hydrates formed within the MOFs were characterized using HRPD and inelastic neutron scattering (INS). The hydrophilic MIL-100 (Fe) MOF was reported to promote the growth of methane hydrates within its internal pores with a lower water-to-hydrate percentage, whereas the hydrophobic ZIF-8 MOF only promoted the growth of methane hydrate within the interparticle space between pores and/or within the peripheral surface area because the hydrophobic inner surface did not permit water to gain access to the internal micropores.

Molecular dynamics (MD) simulations have also been performed to examine the growth kinetic process of methane hydrates within MOFs. Recently, He *et al.* simulated the influence of water content on the formation of methane hydrate and the associated kinetic processes in a mesoporous MIL-101 MOF.¹⁵⁷ MIL-101 is composed of a complex porous network built from 1,4-benzenedicarboxylic acids and octahedral Cr₃O trimers.¹⁶⁴ The cage structures of MIL-101 contribute to the nanopores whereas the inter-particle space of the material provides the meso/macropores. Accordingly, MIL-101 particles have an exceptionally large pore volume and

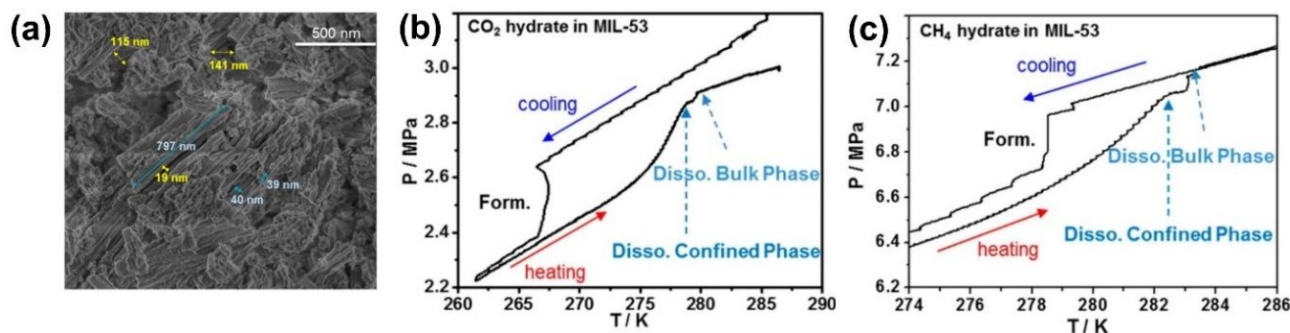


Fig. 8 (a) SEM image of MIL-53; blue and yellow arrows indicate the sizes of the corresponding crystal and void, respectively. P–T trace curves depicting the formation and dissociation of (b) CO₂ and (c) CH₄ hydrates in MIL-53.¹⁵³ Reproduced with permission from Ref.¹⁵³. Copyright 2015, American Chemical Society.

surface area. In this study, methane hydrate was found to form selectively within the exterior area of MIL-101 cavities. Methane molecules within the exterior area were steadily drained following the sustained growth of gas hydrate, and a methane concentration gradient was established between the MIL-101 pore cavities and the exterior area, consequently driving the diffusion of methane molecules out of the pore cavities. Nonetheless, a stable gas hydrate can form within the pore cavities of MIL-101 after the gas hydrate growth within the exterior area was almost full.

In the past decade, studies focusing on the design of suitable organic building blocks through reticular chemistry have paved the way towards the discovery of new water-stable MOF structures with exceptionally high water adsorption capacity.^{165, 166} Following this trend, Cuadrado-Collados *et al.* evaluated Cr-soc-MOF-1 that has high water adsorption capacity (~200 wt.%) for studying the formation of CH₄ hydrates within its porous cavities.¹⁵⁸ Cr-soc-MOF-1 structure consists of chromium trimers together with tetratopic organic building blocks. It has an apparent surface area of 4500 m²/g and pore size of about ~1.6 nm. The CH₄ hydrates were characterized using inelastic neutron scattering, high-pressure methane adsorption measurements, and synchrotron X-ray powder diffraction. In the high-pressure methane adsorption study of Cr-soc-MOF-1, the authors observed that when the cavities were partially or completely saturated with water, CH₄ could not access the inner pores to form hydrates. However, the scenario changed significantly upon going slightly above the oversaturation conditions (~150 wt.%) at 4.5 MPa. Above this pressure threshold, the CH₄ uptake showed a sharp increase of 33 wt.% at >6 MPa. This sudden increase in CH₄ uptake by Cr-soc-MOF-1 was strong evidence of the CH₄ hydrate formation. Additionally, the CH₄ hydrates were also discovered to form in the inner cavities of Cr-soc-MOF-1 because the pressure required for the formation of CH₄ hydrate on the surface and in larger pores was usually at 3–4 MPa.¹²⁶ It was observed that the internal surface chemistry of the pores and porous structures (cuboidal cavities and 1D pore channels of size ~1.6 nm) promoted the formation and nucleation of the sl structure of CH₄ hydrate within the porous network.

3.2 CO₂ Hydrates in MOFs

Owing to the success of applying MOFs to form methane hydrates within their pores, many MOF researchers have started to evaluate the properties of reported water-stable MOFs for CO₂ hydrate storage. One example is the investigation of the HKUST-1 MOF on the storage for N₂, H₂, and CO₂ in the form of gas hydrates (Table 2).¹⁴⁷ HKUST-1 consists of three types of pores. The two bigger pores (1.06 nm and 1.24 nm) are hydrophilic, whereas the small pore (0.5 nm) was comparatively hydrophobic due to the exposed copper.^{167, 168} The gas storage capacity of CO₂ was found to be pressure-dependent, but, for N₂ and H₂, it was severely inhibited because the water-saturated pores significantly reduced the available pore volume of the micropores. When the water-saturated HKUST-1 was exposed to CO₂ (50 bar), new diffraction peaks corresponding to the planes of structure sl CO₂ hydrate were observed. The

samples subjected to only N₂ and H₂ gas (100 bar) showed no difference in diffraction peaks and thus, no gas hydrates were formed. This enhanced CO₂ storage capacity observed at higher pressure (>23 bar) was due to the formation of CO₂ hydrates within the mesopores. The introduction of CO₂ disturbed the adsorbed water molecules within the water-saturated HKUST-1 framework, whereas no difference was detected in the diffraction patterns of the water-saturated HKUST-1 framework when pressurized with N₂ and H₂ separately.

4. Quasi-2D Gas Hydrates in Graphene Nanoslits

Recent studies of materials growth confined to *quasi*-two-dimensional (Q-2D) space such as slits between surfaces (sometimes referred to as slit nanopores) have guided the discovery of many novel 2D materials possessing unusual chemical and physical properties.^{169, 170} Presently, no structures of Q-2D gas hydrates have been experimentally verified, conjectures of the existence of these materials can be inferred by the theoretical predictions of Q-2D polymorphs of ice at low temperatures. Since the first reported simulation proof of the spontaneous growth of bilayer ice enclosed within the sub-nanometer gap of a graphene slit nanopore¹⁷¹, many new Q-2D polymorphs of ice such as monolayer^{172, 173}, bilayer^{174, 175}, and trilayer^{176, 177} polymorphs within hydrophobic slit nanopores have been revealed using MD simulations as well as through experiments.¹⁷⁸ In the laboratory, the formation of the bilayer ice I has been also realized through vapor deposition at extremely low temperatures on a graphene/Pt(111) substrate or an Au(111) substrate.^{178, 179} The first simulation evidence of the spontaneous formation of 2D monolayer argon hydrate within hydrophobic nanoslit was reported by Bai *et al.* in 2010.¹⁷² Even though the spontaneous growth of two-dimensional clathrate hydrates has been reported previously using MD simulation, the molecular insight, and growth mechanism of such low-dimensional gas hydrates are yet fully understood.¹⁸⁰⁻¹⁸²

4.1 Q-2D H₂ Hydrate in Graphene Nanoslits

The first MD simulation evidence of the Q-2D H₂ hydrates was reported by Zhao *et al.* They found that H₂ rapidly formed a bilayer (BL) hydrate within the nanoslits between parallel graphene sheets (Fig. 9 and Table 3).^{183, 184} The hexagonal hydrate crystal with single occupancy of an H₂ molecule in each hexagonal cage was demonstrated to be the thermodynamically stable phase. The size effect of the guest gas molecule on the formation of the BL gas hydrates within the nanoslits was also investigated using ethane (C₂H₆), ethene (C₂H₄), allene (C₃H₄), carbon dioxide (CO₂), and hydrogen (H₂). Apart from these gases, NH₃ and H₂S were also studied since both molecules exhibit strong intermolecular hydrogen-bonding with water. Several stable BL gas hydrate structures with either the nonpolar or polar nature of guest gas molecules confined within a nanoslit were observed. The structures of the hydrate cages depended on the size of the guest gas molecule. Additionally, bigger guest gas molecules were observed to induce the formation of larger cages for the corresponding

structures of the BL hydrates. In the cases of guest gas molecules bigger than CO_2 such as CH_4 ,¹⁷⁵ or linear molecules such as C_2H_6 , C_2H_4 , and C_3H_4 , the BL-square-octagonal clathrate hydrate structures were observed. Also, for polar guest molecules such as NH_3 and H_2S , they were found capable of displacing water molecules from the actual lattice sites of the whole water framework in the BL hydrate structures. NH_3 and H_2S both act as hydrate promoters that strengthen the hydrate cage by extending the hydrogen bonding network and subsequently causing the formation of larger water cages.

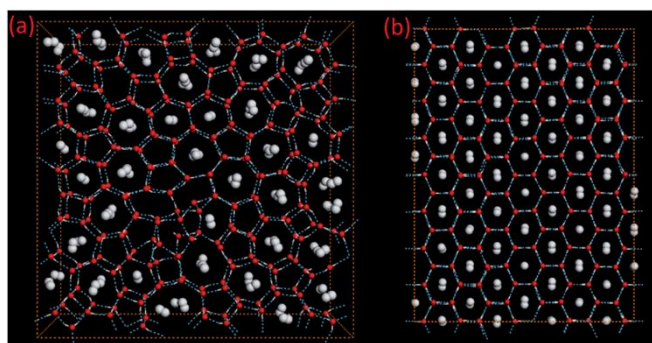


Fig. 9 Simulated models of (a) BL amorphous H_2 hydrate and (b) constructed perfect BL-hexagonal H_2 hydrate. Red spheres represent oxygen. Small white spheres represent the hydrogen of water, whereas big white spheres represent hydrogen molecules. Blue dotted lines indicate hydrogen bonds.¹⁸⁴ Reproduced with permission from Ref.¹⁸⁴. Copyright 2015, Royal Society of Chemistry.

Motivated by the MD simulation results of BL gas hydrates, Zhong *et al.*¹⁸⁵ applied first-principles quantum chemistry calculations to examine the structural characteristics and thermodynamic phase stability of Q -2D H_2 hydrates (Table 3). Four new BL H_2 hydrate structures were predicted by density functional theory (DFT) calculations.¹⁸⁵ This Q -2D H_2 hydrate confined within graphene sheets exhibited superior H_2 storage capacity in comparison to that of bulk THF- H_2 hydrates.¹⁸⁶⁻¹⁹⁴ Interestingly, the BL hydrates were found to be highly susceptible to the distance between the graphene sheets but not towards the hydrophobicity of the plates.^{175, 183, 195}

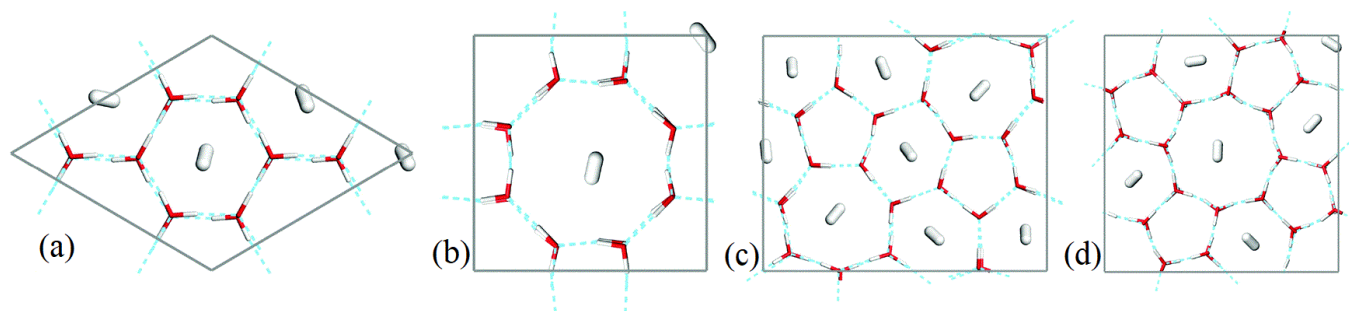


Fig. 10 Structures of Q -2D H_2 hydrates: (a) BLHH-I ($4-6^24^6$) unit cell, (b) BLHH-II ($2-4^6, 2-8^24^8$) unit cell, (c) BLHH-III ($2-5^24^5, 6-6^24^6, 2-7^24^7$) unit cell, and (d) BLHH-IV ($4-5^24^5, 4-6^24^6, 2-8^24^8$). The water and hydrogen molecules are shown as stick models.¹⁸⁵ Reproduced with permission from Ref.¹⁸⁵. Copyright 2020, PCCP Owner Societies.

To study the effect of the space between the graphene sheets on the structure of Q -2D H_2 hydrates, geometry optimization was applied to optimize the structures of the hydrates enclosed within two graphene sheets with a separation distance from 8.0 Å to 11.0 Å. Here, the notation used to denote a hydrate cage is $X^aY^b\cdot m\text{H}_2$. “X” and “Y” represent the shape or geometry of the water cage in the lateral and vertical direction, respectively, whereas “a” and “b” indicate the number of water rings differently. The symbol “m” denotes the number of hydrogen gas molecules entrapped within the hydrate cages. When the distance between two graphene sheets was 9.0 Å, the optimized hydrate structures with singly H_2 -occupied cages had the highest stability with the different structures following the stability order of $6^24^6\cdot\text{H}_2 > 8^24^8\cdot\text{H}_2 > 7^24^7\cdot\text{H}_2 > 5^24^5\cdot\text{H}_2$. For hydrate structures with doubly H_2 -occupied cages, the optimized distance between the graphene sheets for the maximum stability hydrate cages was found to be 9.2 Å. Comparing the hydrate structures with triply and quadruply- H_2 occupied cages, the 8^24^8 structure had the highest stability. Due to the space constraints, four novel hydrate structures, namely BLHH-I ($4-6^24^6$), BLHH-II ($2-4^6, 2-8^24^8$), BLHH-III ($2-5^24^5, 6-6^24^6, 2-7^24^7$), and BLHH-IV ($4-5^24^5, 4-6^24^6, 2-8^24^8$), were observed by DFT optimization (Fig. 10).

4.2 Q -2D CH_4 Gas Hydrates in Graphene Nanoslits

The first MD simulation evidence of Q -2D CH_4 hydrates was the BL CH_4 hydrate reported by Bai and Zeng.¹⁷⁵ Their study started from an initial system of phase-separated liquid water and CH_4 gas, both confined to a nanoslit at 300 K and 10 MPa. When the pressure was increased instantly to 1.0 GPa, nucleation of the CH_4 -containing water octagon was observed at a very early stage. However, the formed octagons kept on collapsing until nuclei of a critical size (consisting of at least four water octagons) were formed. They also computed the melting point of the BL CH_4 hydrate with 100% singly CH_4 -occupied cage at 285 K and ambient pressure.

Following a similar trend, Q -2D CH_4 hydrates were also studied using first-principles quantum chemistry calculations.¹⁹⁶ Different structures of Q -2D CH_4 hydrates were observed after the confinement of water and CH_4 molecules between two parallel graphene sheets with a separation distance from 8.0 Å to 13.0 Å (Table 3). In this study, two distinct types of CH_4

Table 3 Table showing the cage occupancy and the hydrate cage structures of different Q-2D gas hydrates formed between parallel graphene sheets.

| Guest gas | Hydrate cage | Cage occupancy | Distance between graphene sheets (Å) | Wt % of guest gas | Ref. |
|-------------------------------|---|----------------|--------------------------------------|-------------------|------|
| H ₂ | BL-Hexagonal | Single | 8.0 | - | 184 |
| CO ₂ | BL-Heptagonal | Single | 8.0 | - | |
| C ₂ H ₆ | BL-Octagonal | Single | 8.0 | - | |
| C ₂ H ₄ | BL-Octagonal | Single | 8.0 | - | |
| C ₃ H ₄ | BL-Octagonal | Single | 8.0 | - | |
| CH ₄ | X ² ·CH ₄ | Single | 9.0 | - | 196 |
| | (X ² ·CH ₄) ₂ | Double | 11.5 | - | |
| | (X ² ·CH ₄) _{II} | - | 12.0 | - | |
| H ₂ | BLHH-I (4·6 ² 4 ⁶) | - | 9.0 | 2.703 | 185 |
| | BLHH-II (2·4 ⁶ , 2·8 ² 4 ⁸) | - | 9.0 | 1.37 | |
| | BLHH-III (2·5 ² 4 ⁵ , 6·6 ² 4 ⁶ , 2·7 ² 4 ⁷) | - | 9.0 | 2.174 | |
| | BLHH-IV (4·5 ² 4 ⁵ , 4·6 ² 4 ⁶ , 2·8 ² 4 ⁸) | - | 9.0 | 1.639 | |

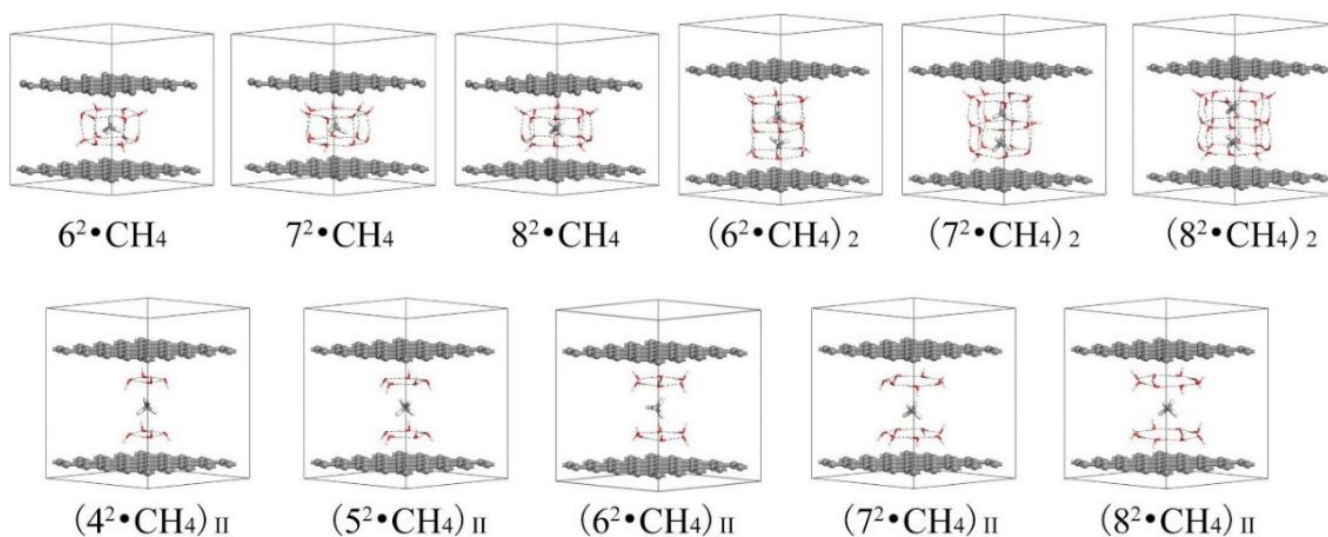


Fig. 11 Geometry optimized structures of Q-2D CH₄ hydrates confined between two parallel graphene sheets. The water and methane molecules are shown in the stick model, the C atoms are shown in a ball-and-stick model, and the hydrogen bonds are shown in dashed black lines.¹⁹⁶ Reproduced with permission from Ref.¹⁹⁶. Copyright 2019, Elsevier Publishers.

hydrate cages, the “plum-pudding” and the “sandwich” cages were reported. In the “plum-pudding” structure, the adjacent water molecules formed a singly CH₄-occupied cage. For the “sandwich” cage structure, the water molecules formed two planar water ring layers “sandwiching” a CH₄ molecule. The structures of the three cage patterns were denoted by the notation (Xⁿ·CH₄)_m, where “X” denotes the number of water molecules in a single planar water ring, the superscript “n” denotes the number of layers of water, and the superscript “m” denotes either the number of coplanar cages or the “sandwich” cage structure (II).

Overall, the three cage patterns were predicted to follow the stability order of X²·CH₄ > (X²·CH₄)₂ > (X²·CH₄)_{II}. The “plum pudding” hydrate structures containing the single-cage X²·CH₄ structures (X = 6 - 8) had the highest stability when the gap between the two graphene sheets was 9.0 Å (Fig. 11). The relative stability of the three similarly “plum pudding” hydrate structures follows the trend: 8²·CH₄ > 7²·CH₄ > 6²·CH₄ (Fig. 11). The 8²·CH₄ cage formed within two graphene sheets having a separation distance of 8.0 - 12.0 Å, whereas the 6²·CH₄ and 7²·CH₄ hydrate cages formed readily with the distance between the graphene sheets to be at least 8.5 Å. The other “plum pudding” hydrate structures contained coplanar double cages. The coplanar double cage (X²·CH₄)₂ structures (X = 6 - 8) formed when the separation distance between the two graphene sheets was 11.5 Å (Fig. 11). The stability of these hydrates with coplanar double cages followed the order: (8²·CH₄)₂ > (7²·CH₄)₂ > (6²·CH₄)₂. In comparison to the single cage X²·CH₄, double cages (X²·CH₄)₂ exhibited less stability. To obtain stable (X²·CH₄)_{II} (X = 4 - 8) “sandwich” cage hydrate structures, the optimum distance between the two graphene sheets was found to be 12.0 Å. The order of the stability of different sandwich methane hydrate structures was (5²·CH₄)_{II} > (4²·CH₄)_{II} > (6²·CH₄)_{II} > (7²·CH₄)_{II} > (8²·CH₄)_{II}.

5. Quasi-1D Gas Hydrates in Carbon Nanotubes

Carbon nanotubes (CNTs) have been explored to provide quasi-one-dimensional (Q-1D) channels for growing gas hydrate. There are two types of CNTs, single-walled carbon nanotubes (SWCNTs) and multi-walled carbon nanotubes (MWCNTs). SWCNTs are often regarded as a rolled-up infinitely long graphene sheet with a set of opposing edges chemically bonded to each other (Fig. 12).^{197, 198} MWCNTs are composed of concentric, nesting shells of SWCNTs like matryoshka Russian dolls (Fig. 12).

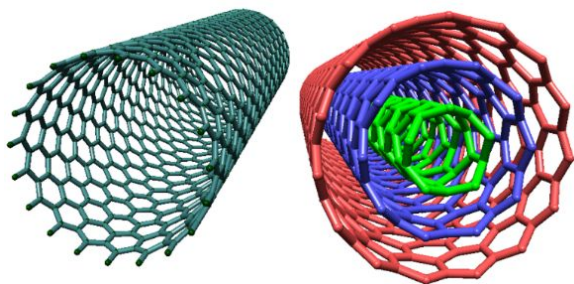


Fig. 12 Schematic representations of (left) a single-walled carbon nanotube (SWCNT) and (right) a multi-walled carbon nanotube (MWCNT).

Studies of gas hydrates in SWCNTs were inspired by the widespread interests in the structure of water in a restricted environment¹⁹⁹, in its degree and type of hydrogen bonding²⁰⁰⁻²⁰⁴, and proton transfer via “water wires”.^{205, 206} The formation of gas hydrates in SWCNTs was first reported by Tanaka and Koga²⁰⁷ using classical molecular dynamics (MD) and grand canonical Monte Carlo (GCMC) simulations. Their results revealed that these hydrates adopt structures containing an octagonal ice nanotube with a hollow space filled with hydrophobic guest gas molecules such as neon, argon, and methane. The attractive interactions between the guest gas molecules and the nanotube ice and the SWCNTs were found to stabilize the structures.

5.1 Q-1D H₂ Hydrate in SWCNTs

Inspired by the success of Tanaka and Koga,²⁰⁷ Zhao *et al.* applied both MD and *ab initio* molecular dynamics (AIMD) simulations to verify the formation of H₂ hydrate inside SWCNTs of various diameters.²⁰⁸ Significantly, they observed the rapid growth of Q-1D H₂ hydrates at near ambient temperature and pressure. Similar to the results of Tanaka and Koga,²⁰⁷ inside the SWCNTs, the guest H₂ molecules in the Q-1D gas hydrates form a chain of molecules inside polygonal ice nanotubes (Fig. 13).

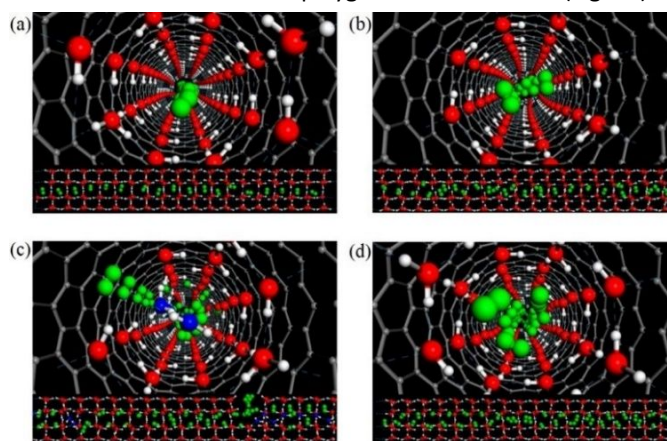


Fig. 13 Axial views (top panels) and side views (bottom panels) of the inherent structures of the Q-1D octagonal H₂ hydrates formed in (17, 0) SWCNT.²⁰⁸ Reproduced with permission from Ref.²⁰⁸. Copyright 2014, American Chemical Society.

The structures, composition, and stability of H₂ hydrates inside SWCNTs were revealed to be highly dependent on the diameters of the SWCNTs. For the (14, 0), (15, 0), (16, 0), and (17, 0) SWCNTs, their diameters vary from 1.09 nm to 1.33 nm, and their corresponding spontaneous formation of pentagonal, hexagonal, heptagonal, and octagonal H₂ hydrates was observed (Table 4). As the size of the ice nanotubes increased, the H₂O/H₂ ratios of these Q-1D H₂ hydrates also increased from 5:1 to 8:1. Computed basis set superposition error (BSSE) corrected interaction energy values between the H₂ molecule and polygonal ice nanotube were applied to calculate the structural stability of these novel gas hydrate structures. At the formation temperature, if the interaction energy values were positive, H₂ molecules could simply escape the polygonal H₂ hydrate structure if the SWCNT was open-ended, and much

larger pressure was required to capture H₂ molecules within this SWCNT system. For example, for the (15, 0) SWCNT system, the interaction energy was about -0.09 eV, indicating that it was energetically favorable for the H₂ molecules to be encapsulated within the hexagonal ice nanotube. The AIMD trajectories also showed that in the larger (17, 0) SWCNT, stable octagonal H₂ hydrates having either single or double occupancy per octagon prism were possible at 250 K. Overall, the predicted growth conditions of H₂ hydrates at near ambient temperature and pressure in water-filled SWCNTs make this material very attractive as a potential hydrogen storage material.

5.2 Q-1D CO Hydrate in SWCNTs

The formation of Q-1D carbon monoxide (CO) hydrate within SWCNTs was reported by Zhao *et al.*²⁰⁹ at ambient pressure (Table 4). Similar to the case of Q-1D H₂ hydrates,²⁰⁸ the structure of this CO hydrate was composed of a polygonal ice nanotube containing a chain of CO molecules in the centre. In this study, they studied the selective adsorption of CO by the ice nanotubes in presence of H₂. They observed selective adsorption of CO over H₂ molecules in octagonal and nonagonal ice nanotubes. The water to CO gas ratio in these nanotube CO hydrates was also found strongly dependent on the sizes of SWCNTs. For example, heptagonal gas hydrate was formed rapidly in the (17, 0) SWCNT at 280 K (Table 4). In this case, this hydrate permitted only an average of 1.3 CO and 2.2 H₂ molecules to diffuse through. Thus, the heptagonal gas hydrate was undesirable for separating a mixture of CO and H₂. In contrast, the (18, 0) and (19, 0) SWCNTs were predicted to readily allow the guest molecules to diffuse. The octagonal gas hydrate in (18, 0) SWCNT allowed the diffusion of 8.4 CO and 0.8 H₂ molecules. The mean quantity of CO molecules diffused through the nonagonal nanochannel of gas hydrate inside the (19, 0) SWCNT was increased to around 9.0, whereas the number of H₂ molecules was just 0.8. This suggests that the nonagonal gas hydrate may better suit to separate the CO and H₂ molecules in diluted CO/H₂ aqueous solutions. The preferential adsorption of CO over H₂ within the ice nanotube can be applied to design a process for purifying hydrogen.

5.3 Q-1D CO₂ Hydrate in SWCNTs

The simulation proof of the existence of Q-1D polygonal (7-, 8-, and 9-gonal) CO₂ hydrates inside SWCNTs was investigated by Zhao *et al.*²¹⁰. As shown in Fig. 14, the Q-1D heptagonal and octagonal CO₂ hydrates were formed rapidly within (17, 0) and (18, 0) SWCNTs, whereas the growth of the nonagonal CO₂ hydrate was observed within a (19, 0) SWCNT. Highly selective adsorption of CO₂ over H₂ gas molecules was also observed in Q-1D hydrates within SWCNTs. This was attributed to the lower free energy profile of CO₂ diffusing from the bulk solution into the polygonal ice nanotube than that for H₂. Similar to the case of CO hydrates, the high preferential selectivity of CO₂ over H₂ in a dilute CO₂/H₂ aqueous solution was found dependent on the diameter of the SWCNTs rather than their chirality. The modeling results of the selective adoption study revealed that numerous CO₂ gas molecules and some H₂ gas molecules were encapsulated within the Q-1D polygonal gas hydrates. For

example, the heptagonal hydrate in a (17, 0) SWCNT trapped CO₂ and H₂ in the ratio of *ca.* 5.8 on average. The average ratio of trapped CO₂/H₂ for the octagonal hydrate in an (18, 0) SWCNT was about 11, whereas that for the nonagonal hydrate in a (19, 0) SWCNT was about 15.

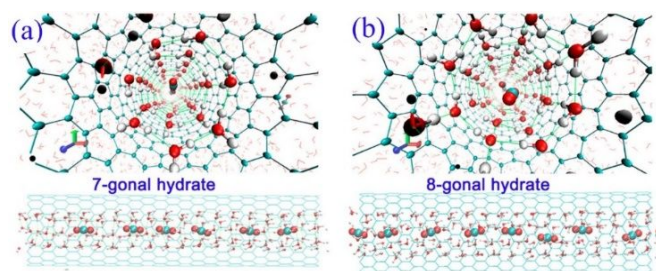


Fig. 14 Axial views (top panels) and side views (bottom panels) of snapshots of the Q-1D (a) heptagonal and (b) octagonal CO₂ hydrates in SWCNTs.²¹⁰ Reproduced with permission from Ref.²¹⁰. Copyright 2018, American Chemical Society.

5.4 Q-1D CH₄ Hydrates in SWCNTs

The formation of Q-1D CH₄ hydrates was reported in SWCNTs of different sizes using MD simulation (Fig. 15 and Table 4).²¹¹ However, unlike the cases of H₂, CO, and CO₂ hydrates, CH₄ hydrates formed only when a few of the water molecules of ice nanotubes were substituted by CH₄. The results were explained by the stronger methane-CNT interactions than the water-CNT interactions and the great propensity of water molecules to form hydrogen bonds. The results also matched the findings of Tanaka *et al.*,²⁰⁷ in which the interactions of the guest molecules with the ice nanotube in the SWCNTs were observed to affect the stability and structure of gas hydrates. Although the types of ice nanotubes of CH₄ hydrates formed in SWCNTs were similar to H₂ hydrates, their structural distributions were different. In the (13, 0), (14, 0), and (15, 0) SWCNTs, there was one layer of water molecules formed before the addition of methane molecules, but two layers were formed following the addition of the methane molecules. Nevertheless, in the (16, 0) and (17, 0) SWCNTs, two layers of water molecules were formed, but three or more water layers were formed following the addition of the methane molecules.

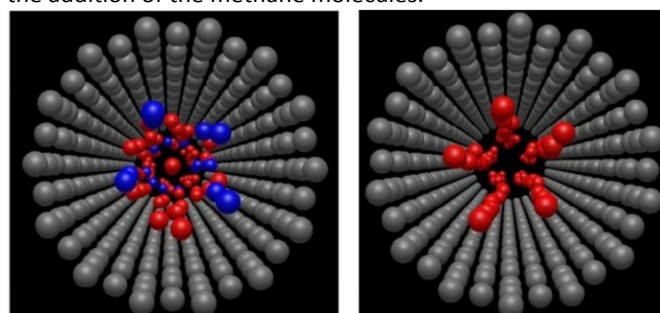


Fig. 15 The formation of methane hydrates in the (14,0) SWCNTs in the states of (left) "with methane" and (right) "without methane". Water molecules are in red and methane molecules are in blue.²¹¹ Reproduced with permission from Ref.²¹¹. Copyright 2018, Centre National de la Recherche Scientifique (CNRS) and The Royal Society of Chemistry.

The structural stability of methane hydrates formed in SWCNTs can also be understood from the self-diffusion coefficients of water molecules within the nanotube models with and without CH₄ (Fig. 15).²¹¹ In the absence of CH₄, the self-diffusion constants of water molecules in water-filled SWCNTs were relatively large (0.158–0.250 × 10⁵ cm² s⁻¹), indicating that the ice nanotubes formed in the SWCNTs were liquid-like. However, in the presence of CH₄, the self-diffusion constants of water molecules dropped by 50% to 90% in values. For the (16, 0) SWCNT, the self-diffusion constants of water molecules of the methane hydrates were the smallest among the computed results. This observation was attributed to the rise in the total number of molecules with an increase in the accessible SWCNT volume and the formation of two rows of water molecules in

the middle of the carbon nanotube instead of only polygonal ice nanotubes.

5.5 Q-1D N₂ Hydrates in SWCNTs

The simulation proof of the existence of Q-1D nitrogen (N₂) hydrate inside SWCNTs was investigated by Li *et al.*²¹² They demonstrated an electric-field-triggered process to release N₂ molecules from the hydrate structure. The role of the electric field in this gas release process was to interrupt the hydrogen-bonding network of the ice nanotube, resulting in the change of diffusion coefficient of the water molecules in the hydrate structure. In this study, N₂ diffused into the SWCNT and formed Q-1D N₂ hydrate when they were initially placed randomly in the bulk water. An octagonal structure (type A) of Q-1D N₂ was

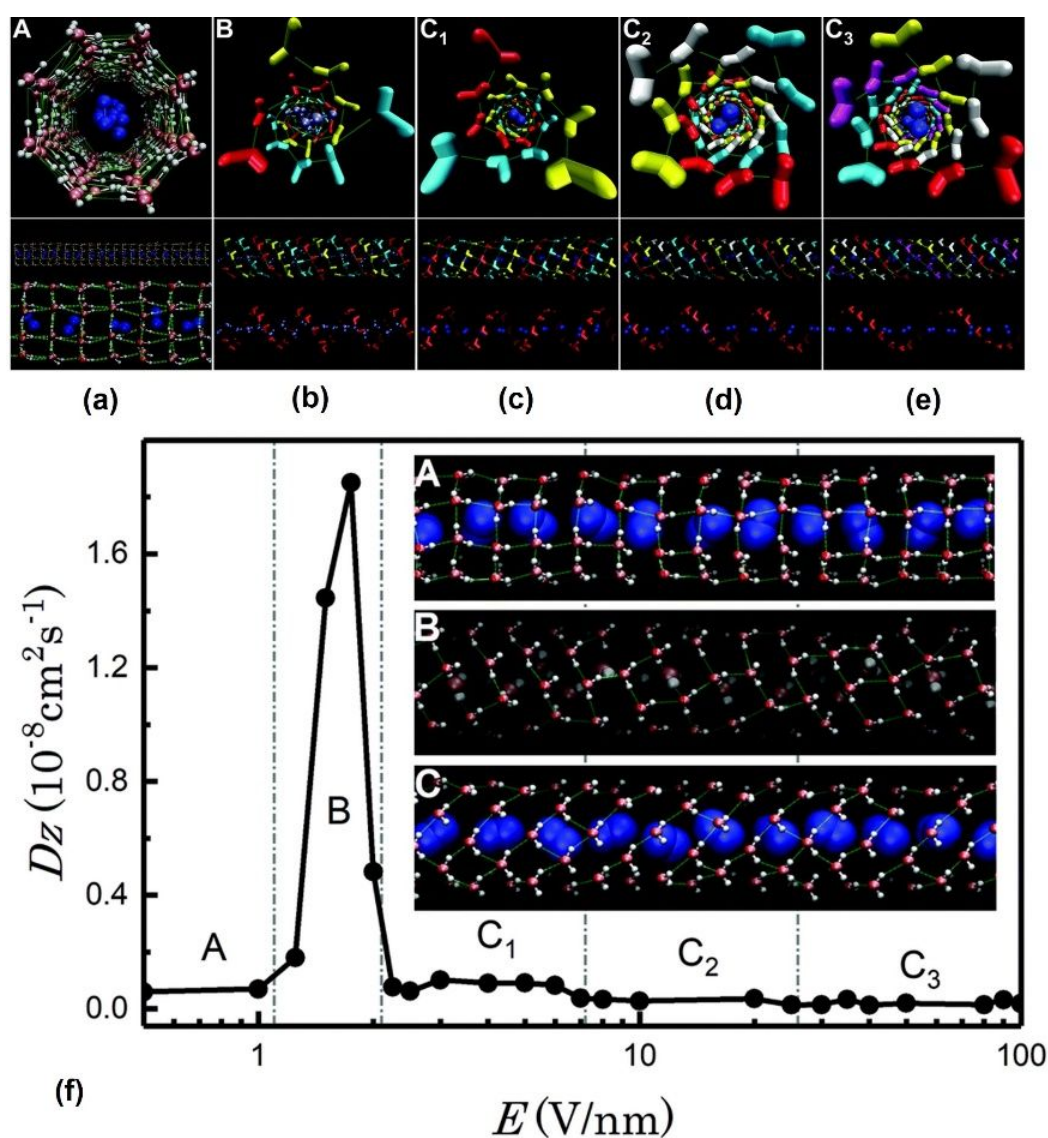


Fig. 16 Schematic showing 5 structures of Q-1D N₂ hydrates formed in SWCNT under the electric field. (a) An octagonal N₂ hydrate (type A). (b) A gas-free helical hydrate (type B). (c) A helical N₂ hydrate (type C₁). (d) A helical N₂ hydrate (type C₂). (e) A helical N₂ hydrate (type C₃). For (a), red, pink, and white spheres represent oxygen and hydrogen atoms, respectively. For (b)–(e), red, yellow, cyan, white, and violet licorices represent different helices of the water chain. Blue spheres and ice blue spheres represent N₂ molecules and water molecules in the center, respectively. (f) The diffusion coefficient of water is a function of the electric field (E). White, red, and blue spheres represent hydrogen, oxygen, and nitrogen atoms, respectively. Lime dotted lines denote hydrogen bonds.²¹² Reproduced with permission from Ref.²¹². Copyright 2020, Royal Society of Chemistry.

Table 4 Physical properties of different Q-1D gas hydrates formed inside single-walled carbon nanotubes (SWCNTs).

| Guest Gas | SWCNT Index | Diameter (nm) | Gas Hydrate Geometry | Water/Guest ratio | Wt. % of guest gas | T _{formation} (K) | Ref. |
|-----------------|-------------|---------------|-------------------------|-------------------|--------------------|----------------------------|------|
| H ₂ | (14,0) | 1.09 | 5-gonal | 5:1 | 0.37 | 290 | 208 |
| | (15,0) | 1.17 | 6-gonal | 6:1 | 0.34 | 390 | |
| | | | Phase-separated | <6:1 | - | - | |
| | (16,0) | 1.25 | 6-gonal | 6:1 | 0.33 | 300 | |
| | | | Mixed (7-gonal/6-gonal) | (6:1, 7:1) | (0.32, 0.33) | - | |
| | | | 7-gonal | 7:1 | 0.32 | 400 | |
| | (17,0) | 1.33 | 7-gonal | 7:1 | 0.30 | 330 | |
| | | | Mixed (8-gonal/7-gonal) | (7:1, 8:1) | (0.29, 0.30) | - | |
| | | | 8-gonal | 8:1 | 0.29 | 330 | |
| | | | | (8:1, 8:2) | (0.29, 0.58) | | |
| | | | 8:2 | 0.58 | 410 | | |
| CO | (17,0) | 1.33 | 7-gonal | <8:1 | - | 280 | 209 |
| | (18,0) | 1.41 | 8-gonal | 10:1 | - | 270 | |
| | (19,0) | 1.49 | 9-gonal | 9:1 | - | 270 | |
| CO ₂ | (17,0) | 1.33 | 7-gonal | 5.8:1 | 2.43 | 260 | 210 |
| | (18,0) | 1.41 | 8-gonal | 11:1 | 2.36 | 260 | |
| | (19,0) | 1.49 | 9-gonal | 15:1 | 3.23 | 240 | |
| CH ₄ | (13,0) | 1.01 | 4-gonal | - | - | 250 | 211 |
| | (14,0) | 1.09 | 5-gonal | - | - | 250 | |
| | (15,0) | 1.17 | 6-gonal | - | - | 250 | |
| | (16,0) | 1.25 | 7-gonal | - | - | 250 | |
| | (17,0) | 1.33 | 8-gonal | - | - | 250 | |
| N ₂ | (17,0) | 1.35 | 8-gonal | 10:1 | - | 240 | 212 |

observed (Fig. 16(a) and Table 4). An N_2 wire occupied the hollow space within the octagonal ice nanotube. The effect of the electric field (E) on the behavior of the Q -1D hydrate confined in SWCNT was studied by analyzing the axial diffusion coefficient (ADC) of water in the Q -1D hydrate under different electric fields (Fig. 16(f)). For $E = 0$, the ADC of water in SWCNT was $7.3 \times 10^{-10} \text{ cm}^2 \text{ s}^{-1}$. For $0 < E \leq 1 \text{ V nm}^{-1}$, the ADC of water remains constant, but the orientation of the water molecules changed from bipolar orientation to uniform orientation. In the range of $1 \leq E \leq 1.25 \text{ V nm}^{-1}$, the octagonal ice nanotube structures transform into a helical structure called type B (Fig. 16(b)). Simultaneously, the N_2 molecules are released from the helical ice tube and are displaced by a single water chain (see Fig. 16(b)). Furthermore, the ADC increased significantly when E was in the range of $1.25 \leq E \leq 2 \text{ V nm}^{-1}$. With an increasing value of E , interestingly, the ADC of water dropped sharply to the magnitude of $\sim 10^{-10} \text{ cm}^2 \text{ s}^{-1}$. For the range of $2.25 \leq E \leq 100 \text{ V nm}^{-1}$, the N_2 molecules were encapsulated by an ordered helical ice nanotube (type C). Additionally, the type C structure can further be divided into type C1, C2, and C3, corresponding to the three new structures of the ice nanotubes. In the type C1 structure, the structure of the ice nanotube (hydrate shell) is similar to that of the type B structure (Fig. 16(c)). For type C2 and C3 structures, there are four and five helical water chains respectively (Fig. 16(d)-(e)). In the case of type C (C1, C2, and C3), N_2 molecules cannot escape from the helical ice nanotube structure.

5.6 CH_4 Hydrate in MWCNTs

Multi-walled carbon nanotubes (MWCNTs) which are composed of two or more concentric carbon nanotubes have also been explored for the formation of CH_4 hydrates. So far, there has been only one published study on the formation of CH_4 hydrates within MWCNTs through studying the sorption behavior of CH_4 inside water-filled MWCNTs (Fig. 17).²¹³ The existence of water in the MWCNTs was reported to cause the amount of CH_4 adsorbed to be nearly zero at lower pressures. However, the CH_4 adsorption isotherm soared to a higher value at about 3.9 MPa of CH_4 . The equilibrium amount of CH_4 stored in MWCNTs was dependent on their water content. The maximum methane storage was observed when the weight ratio of water to MWCNTs (R_w) was one. The highest quantity of CH_4 stored per unit mass of MWCNTs was 5.1 times higher than those of dry samples. Since the pressure required for the formation of bulk CH_4 hydrate in water was 3.23 MPa,²¹⁴ the increase in the sorption amount of CH_4 in water-filled MWCNTs was probably because of the formation of CH_4 hydrate.

The study concluded that the observed CH_4 hydrate was formed not merely in the pores of MWCNTs but also within the outer spaces present in between the sorbent particles. Nonetheless, MWCNTs were unlikely to be used as a CH_4 storage material because their maximum storage capacity was still less than the other storage methods.

6. Conclusion and Outlook

This review surveys four categories of nanoporous materials

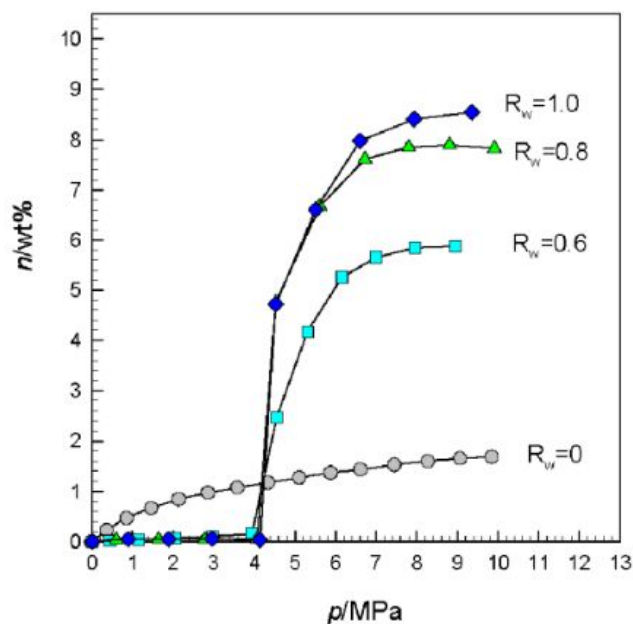


Fig. 17 Methane isotherms on dry and water-filled multi-walled carbon nanotubes (MWCNTs) at 275 K.²¹³ R_w is the weight ratio of water to nanotubes. Reproduced with permission from Ref.²¹³. Copyright 2005, Elsevier Publishers.

including porous carbons, metal-organic frameworks (MOFs), graphene nanoslits, and carbon nanotubes for investigating the formation of gas hydrates in confined spaces. From being traditionally considered a source of troubles in flow assurance, gas hydrates are now regarded as potential chemicals for applications such as gas separation, energy storage and transport, water desalination, and carbon sequestration. However, the requirements of high pressure and slow formation kinetics limit the practical application of bulk gas hydrates. Porous nanomaterials provide promising hosts to facilitate the growth of gas hydrates and drastically improve their formation kinetics. Experimental studies of these materials have revealed a new understanding of the unusual phase behavior of gas hydrates formed under nanoscale confinement. The effectiveness of gas hydrate formation in these materials is dependent on the size of spatial confinement, pore size, sizes of guest gas molecules, and chemical interactions of the materials/media with edges and/or functional groups with gas and water molecules. Although advances in theoretical modeling have yielded numerous new predictions of low-dimensional gas hydrate structures, most of these novel structures discussed in this review lack concrete experimental results. Thus, this review is expected to rekindle researchers' interests in gas hydrate research and encourage them to explore new frontiers of porous materials for the growth of gas hydrates.

Activated porous carbons are composed of ordered micropores with walls of defective graphene-like layers. Owing to their highly nanoporous structure and large internal surface area, water-filled activated porous carbons are promising materials to store gas in the gas hydrate form. For example, the amount of methane stored in pre-humidified carbons at

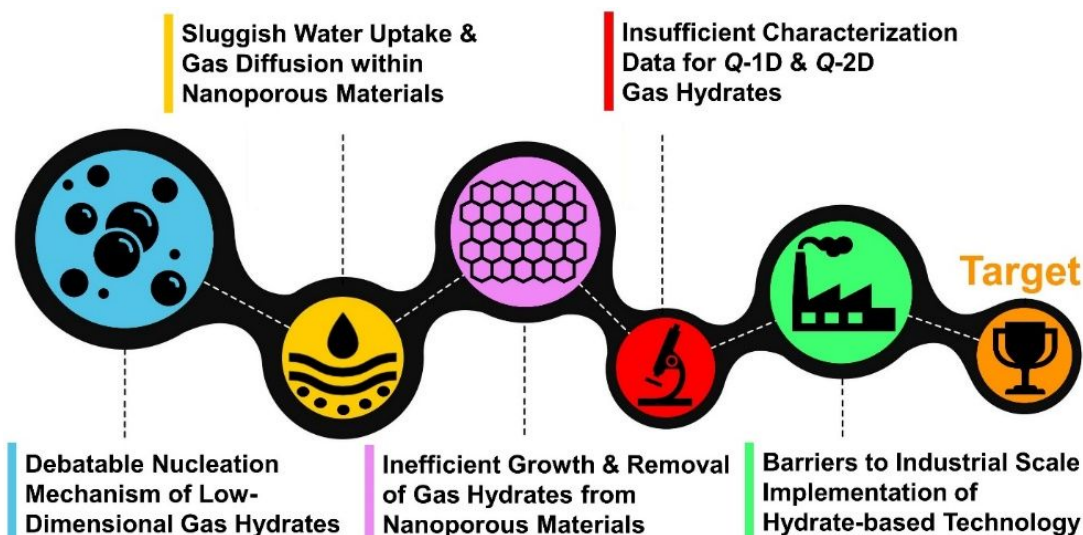


Fig. 18 Current challenges in the development of gas hydrates in confined spaces are depicted in this graphic illustration.

moderate pressure (*ca.* 10 MPa²¹⁵) surpasses the amount stored in the corresponding dry materials considerably.¹²⁵ The hydrophobic pores have been demonstrated to be effective in nucleating gas hydrates. Significantly, activated porous carbons can accelerate the formation kinetics of methane hydrates from days to minutes¹²⁶, making this carbon material the most promising materials for methane storage.

Gas hydrate studies using MOFs²¹⁶ as confined structures demonstrate the complexity of the gas hydrate nucleation and growth process in porous frameworks. MOFs with hydrophobic inner surfaces have been shown to promote the formation process of gas hydrates with a high yield. The controls of the nucleation, formation kinetics, and structures of gas hydrates inside MOFs were found to depend on (i) the structures of the MOF hosts, (ii) the inner surface chemistry, and (iii) the growth conditions.^{145, 217} Owing to the high degree of chemistry control in the design of MOFs, they are promising candidates to initiate the formation of artificial gas hydrates for demanding industrial applications such as gas storage or large-distance gas transport.

Theoretical modeling has predicted the formation of novel gas hydrate structures within graphene nanoslits made of parallel graphene sheets and also within single-walled carbon nanotubes. These unique low-dimensional hydrates not only enrich the gas hydrate family but also provide new model systems towards understanding the formation of gas hydrates in sandy sediments that occur naturally in the environment. Significantly, these low-dimensional gas hydrates with controllable physicochemical features form at ambient pressure and temperature, rendering them potentially important for industrial applications. Nevertheless, the existence of these two novel low-dimensional gas hydrates has yet to be experimentally verified.

Many questions on the nucleation and growth of nanospace-confined gas hydrates and the development of versatile nanoporous materials remain unaddressed. Below we list five major challenges (Fig. 18) in the research of gas hydrates in nanoscale confinements of nanomaterials:

Debatable nucleation mechanism of low-dimensional gas hydrates

- Current nucleation pathways for gas hydrates in nanoconfined porous materials remain under debate. The complexity of this subject lies in the existence of multiple competing pathways that intricately depend on the density, size, volume, shape, and chemical nature of the pores.²¹⁸ Such parameters can affect how the nanoscale confinement intrinsically influences the phase boundaries of gas hydrates. One major challenge in studying the growth of low-dimensional gas hydrates is to achieve sufficient control of gas diffusion into and out of the nanomaterials. Factors such as uniformity of the pores and porosity within the nanoporous materials and the degree of opening of these pores for accessibility can drastically influence the measured nucleation rate and kinetics of hydrate growth.²¹⁹

Sluggish water uptake and gas diffusion within nanoporous materials

- Enhancing the water-gas interphase through the use of porous materials has been demonstrated to initiate hydrate growth. However, the induction time for the hydrate growth in these porous materials is still in the order of hours. Accelerating or regulating the water uptake and gas diffusion within the pores through other external driving forces has the potential to significantly improve the hydrate growth process. Recently, the application of electric field for manipulating the surface wettability²²⁰ of water has been widely used in designing pH-filters,²²¹ oil-water mixtures,²²² liquid droplet actuators,^{223, 224} liquid lenses,²²⁵ and display devices.²²⁶ This observed phenomenon is called electrowetting in which an electric field is used to modify the surface tension between a solid surface and water, resulting in the modification of the wettability and contact angle of water on solid surfaces.²²⁷ Controlling the surface wettability is essential for designing

and fabricating devices such as microfluidics, self-cleaning surfaces, bio-sensors, and filtration devices.²²⁸ Many studies have reported that through modification of water-surface interaction via electrowetting²²⁹, the water uptake^{230, 231} can be regulated and the opening and the closing of pores²³²⁻²³⁴ of different porous materials can even be controlled.²³⁵ Currently, the application of electric field for studying gas hydrate growth in porous nanomaterial has only been modeled by Li et al.²¹²

- The major limitation of most MOFs for confined gas hydrate growth is the collapse of their micropores in the presence of water.²³⁶⁻²⁴⁰ This is attributed to the labile nature of many metal-oxygen bonds which are susceptible to hydrolysis that can cause irreversible destruction of the frameworks. Recent synthetic advances have led to the development of new water-stable MOFs that are suitable for water-sensitive applications such as water-harvesting in arid regions.^{241, 242} These water-stable MOFs show great promises as hosts for growing gas hydrates within their porous structure. Nonetheless, it is still a challenge to anticipate a priori for any new MOF-confined hydrates to overpass the performance of corresponding dry materials. New metal-ligand chemistry is required to improve the storage capacity of the MOF hosts when designing MOFs as nanoreactors to grow artificial gas hydrates.²⁴³ Similar to MOFs, covalent organic frameworks²⁴⁴ (COFs) are hailed as viable candidates²⁴⁵ for studying gas hydrate formation due to their high stability in water, high crystallinity, tunable pore size, large surface area, and unique metal-free molecular architecture. Presently, the research field of COFs is still in its infancy and its application for gas hydrate growth is yet to be explored.^{246, 247}
- In recent years, many studies reported the use of water-stable porous materials such as polymerized high internal phase emulsion (polyHIPE),⁷ “dry water”,²⁴⁸ hydrogels,^{6, 249} and aluminum foams²⁵⁰ to promote the formation of gas hydrates. The high surface areas of these porous materials were observed to accelerate the formation of hydrates probably by enhancing the heat transfer process.⁸⁴ These studies reported high-pressure gas sorption measurements which provided excellent information about the gas uptake. However, they lacked information that could pinpoint whether the gas hydrates were formed within the pores or on the external surface of these porous materials. Nonetheless, these studies demonstrated the promising potential of hydrolytically stable porous polymeric materials.^{7, 251-253} Hence, further exploration of water-stable porous polymeric materials is expected to be a rewarding direction for gas hydrate research.

Inefficient growth and removal of gas hydrates from nanoporous materials

- The different gas storage studies in this review have illustrated that it is still a daunting challenge to reach the DOE target²⁵⁴ of methane storage (180 v/v) with nanoporous materials. This is because the methane storage mechanism within these materials is drastically different

from the bulk. However, in recent years, MOFs have shown great promises in overcoming this hurdle.²⁵⁵ Through optimizing the pore size and pore chemistry by designing specific ligands, the methane storage capacity of MOFs can be significantly enhanced. An ingenious use of the flexibility of MOFs may also enhance their gas hydrate storage capacity. For example, researchers can simply increase the accessible surface area for hydrate growth without increasing the pore volume by using the interpenetration of frameworks in MOFs.²⁵⁶ This strategy may improve the water-gas contact within the pore without changing the pore size. Through developing new synthetic methodologies for MOFs, there would be endless possibilities of different systems fit for the scalable growth of gas hydrates.

- Achieving refined structural control of nanoporous carbon materials can also improve the cycles of gas hydrate formation and dissociation and it is essential for large-scale hydrate production. For example, in the case of SWCNTs, small changes in the nanotube diameter can lead to significant changes in the structures of water tubes inside the SWCNTs and the conductance of these “channels” for gas diffusion. Also, ensuring the opening of the nanotubes and the accessibility of the tubular space in macroscopic samples is necessary for reproducible measurements of the phase change and the formation of gas hydrate inside bulk SWCNTs samples.

Insufficient characterization data for Q-1D and Q-2D gas hydrates

- Advances in computer modeling of gas hydrates in different configurations of nanoscale confined spaces such as nanoslits and nanotubes have led to the predictions of many new gas hydrate structures. Nonetheless, since these structures are highly sensitive to local changes in the host structures, they pose severe challenges in producing samples with extremely uniform nanospace for structural studies using a conventional bulk technique such as X-ray diffraction and neutron diffraction. To verify these theoretically predicted structures, further development of local probe structures characterization techniques such as *in situ* TEM,²⁵⁷ non-contact atomic force microscopy,¹⁷⁸ and confocal infrared spectroscopy,^{258, 259} are recommended for experimental studies of these unique low-dimensional gas hydrate structures.

Barriers to industrial-scale implementation of hydrate-based technology

- The outlooks of gas hydrate research have been shifted from discoveries of new gas hydrates toward developing applications. Presently, most of the reported studies of gas hydrates in nanoporous materials are only conducted in small laboratory-scale reactors. It remains to be demonstrated that laboratory-scale experiments are relevant and representative for gas hydrate applications on large scale. To enable the development of gas hydrates for industrial-scale applications, significant progress in

understanding the gas hydrate growth processes is still necessary to accelerate their scale-up processes. Improved reactor configurations are required to promote faster mass and heat transfer within the nanoporous materials and hence hydrate growth kinetics. These advances are essential to provide sufficient samples for application developments.

- Another novel application of hydrate-based technology is the desalination of seawater. For its large-scale implementation, it is essential to have cost-effective and environmentally sustainable hydrate forming agents. Many explored hydrate forming agents have compromised side effects. For example, sulfur hexafluoride and common refrigerant gases can cause ozone layer depletion. Alkanes are flammable and hence possess safety concerns for large-scale implementation. Recently, studies report that cyclopentane and carbon dioxide are more favorable hydrate forming agents for the desalination process. Cyclopentane can form hydrates at atmospheric pressure, making it an easier system to control at a larger scale.²⁶⁰ Desalination through the carbon dioxide hydrate processing route can serve a dual purpose. CO₂ gas can be captured in the form of CO₂ hydrates from seawater and these hydrates can then decompose to CO₂ gas and potable water.^{43, 79, 261-265} Combining the use of porous materials and hydrate forming agents for the clathrate hydrate-based desalination process has the potential to further alleviate the requirements of high pressure and low temperature. This processing strategy requires efficient separation of the formed hydrate from the porous materials in the water-release process. Linga and co-workers have reported several desalination studies using porous silica systems for growing clathrate hydrate with propane or cyclopentane as co-formers.^{43, 266, 267} In their studies, the clathrate hydrates initially grew at the surface of water-saturated porous materials but then gradually grew out of the pores. Based on these observations, they designed a clathrate hydrate-based desalination apparatus.²⁶⁸ While other porous carbon-based nanomaterials such as carbon nanotubes^{269, 270} and MOFs^{271, 272} have been studied widely for water desalination application, to our best knowledge, their uses as co-hydrate-formers through the hydrate-based desalination approach have yet to be realized.

7. Conflicts of interest

The authors declare no conflict of interest.

8. Acknowledgements

The authors thank the National Science Foundation (Grant #: CHE 1665324) for financial support.

9. References

1. E. D. Sloan Jr, *Nature*, 2003, **426**, 353.
2. C. A. Koh, E. D. Sloan, A. K. Sum and D. T. Wu, *Annu. Rev. Chem. Biomol. Eng.*, 2011, **2**, 237-257.
3. A. Hassanpouryouzband, E. Joonaki, M. Vasheghani Farahani, S. Takeya, C. Ruppel, J. Yang, N. J. English, J. M. Schicks, K. Edlmann, H. Mehrabian, Z. M. Aman and B. Tohidi, *Chem. Soc. Rev.*, 2020, **49**, 5225-5309.
4. H. Davy, *Philos. Trans. Royal Soc.*, 1811, **101**, 1-35.
5. C. Giavarini and K. Hester, *Gas Hydrates: Immense Energy Potential and Environmental Challenges*, Springer Science & Business Media, London, UK, 2011.
6. F. Su, C. L. Bray, B. O. Carter, G. Overend, C. Cropper, J. A. Iggo, Y. Z. Khimiyak, A. M. Fogg and A. I. Cooper, *Adv. Mater.*, 2009, **21**, 2382-2386.
7. F. Su, C. L. Bray, B. Tan and A. I. Cooper, *Adv. Mater.*, 2008, **20**, 2663-2666.
8. E. D. Sloan and C. Koh, *Clathrate Hydrates of Natural Gases*, CRC Press, Boca Raton, FL, USA, 3 edn., 2007.
9. B. Buffett and D. Archer, *Earth Planet. Sci. Lett.*, 2004, **227**, 185-199.
10. A. K. M. Jamaluddin, N. Kalogerakis and P. R. Bishnoi, *J. Petrol. Sci. Eng.*, 1991, **5**, 323-335.
11. E. D. Sloan, C. A. Koh and A. Sum, *Natural Gas Hydrates in Flow Assurance*, Elsevier Science, Burlington, MA, USA, 2010.
12. E. G. Hammerschmidt, *Ind. Eng. Chem.*, 1934, **26**, 851-855.
13. P. Englezos, *Ind. Eng. Chem. Res.*, 1993, **32**, 1251-1274.
14. E. D. Sloan, *Fluid Ph. Equilibria*, 2005, **228-229**, 67-74.
15. T. A. Strobel, K. C. Hester, C. A. Koh, A. K. Sum and E. D. Sloan, *Chem. Phys. Lett.*, 2009, **478**, 97-109.
16. M. D. Max and A. H. Johnson, in *Exploration and Production of Oceanic Natural Gas Hydrate: Critical Factors for Commercialization*, eds. M. D. Max and A. H. Johnson, Springer International Publishing, Cham, Switzerland, 2 edn., 2016, pp. 39-73.
17. P. Englezos and J. D. Lee, *Korean J. Chem. Eng.*, 2005, **22**, 671-681.
18. H. P. Veluswamy, A. Kumar, Y. Seo, J. D. Lee and P. Linga, *Appl. Energy*, 2018, **216**, 262-285.
19. P. Linga, R. Kumar and P. Englezos, *J. Hazard. Mater.*, 2007, **149**, 625-629.
20. S.-P. Kang and H. Lee, *Environ. Sci. Technol.*, 2000, **34**, 4397-4400.
21. P. Babu, P. Linga, R. Kumar and P. Englezos, *Energy*, 2015, **85**, 261-279.
22. C.-G. Xu and X.-S. Li, *RSC Adv.*, 2014, **4**, 18301-18316.
23. X.-S. Li, C.-G. Xu, Z.-Y. Chen and H.-J. Wu, *Energy*, 2010, **35**, 3902-3908.
24. S. Park, S. Lee, Y. Lee, Y. Lee and Y. Seo, *Int. J. Greenh. Gas Con.*, 2013, **14**, 193-199.
25. H. Tajima, A. Yamasaki and F. Kiyono, *Energy*, 2004, **29**, 1713-1729.
26. J. S. Gudmundsson, M. Parlaktuna and A. A. Khokhar, *SPE Prod. & Fac.*, 1994, **9**, 69-73.
27. A. A. Khokhar, J. S. Gudmundsson and E. D. Sloan, *Fluid Ph. Equilibria*, 1998, **150-151**, 383-392.
28. H. Ganji, M. Manteghian, K. Sadaghiani zadeh, M. R. Omidkhah and H. Rahimi Mofrad, *Fuel*, 2007, **86**, 434-441.
29. Z. R. Chong, S. H. B. Yang, P. Babu, P. Linga and X.-S. Li, *Appl. Energy*, 2016, **162**, 1633-1652.
30. T. S. Collett, *AAPG Bull.*, 2002, **86**, 1971-1992.

31. H. Lee, J.-w. Lee, D. Y. Kim, J. Park, Y.-T. Seo, H. Zeng, I. L. Moudrakovski, C. I. Ratcliffe and J. A. Ripmeester, *Nature*, 2005, **434**, 743-746.
32. H. Kanda, presented in part at the 23rd World Gas Conference, Amsterdam, 2006.
33. G. Rehder, R. Eckl, M. Elfgen, A. Falenty, R. Hamann, N. Kähler, W. F. Kuhs, H. Osterkamp and C. Windmeier, *Energies*, 2012, **5**, 2499-2523.
34. N.-J. Kim, J. Hwan Lee, Y. S. Cho and W. Chun, *Energy*, 2010, **35**, 2717-2722.
35. F. Rossi, M. Filippini and B. Castellani, *Appl. Energy*, 2012, **99**, 167-172.
36. Y. Bi, T. Guo, T. Zhu, L. Zhang and L. Chen, *Energy Convers. Manag.*, 2006, **47**, 2974-2982.
37. Y. Xie, G. Li, D. Liu, N. Liu, Y. Qi, D. Liang, K. Guo and S. Fan, *Appl. Energy*, 2010, **87**, 3340-3346.
38. B. Kvamme, A. Graue, T. Buanes, T. Kuznetsova and G. Erslund, *Int. J. Greenh. Gas Con.*, 2007, **1**, 236-246.
39. S. Hirai, Y. Tabe, K. Kuwano, K. Ogawa and K. Okazaki, *Ann. N. Y. Acad. Sci.*, 2000, **912**, 246-253.
40. H. Koide, M. Takahashi, Y. Shindo, Y. Tazaki, M. Iijima, K. Ito, N. Kimura and K. Omata, *Energy*, 1997, **22**, 279-283.
41. J. Zheng, Z. R. Chong, M. F. Qureshi and P. Linga, *Energy Fuels*, 2020, **34**, 10529-10546.
42. K. C. Kang, P. Linga, K.-n. Park, S.-J. Choi and J. D. Lee, *Desalination*, 2014, **353**, 84-90.
43. P. Babu, R. Kumar and P. Linga, *Chem. Eng. Sci.*, 2014, **117**, 342-351.
44. J. Javanmardi and M. Moshfeghian, *Appl. Therm. Eng.*, 2003, **23**, 845-857.
45. C. A. Koh, A. K. Sum and E. D. Sloan, *J. Appl. Phys.*, 2009, **106**, 061101.
46. A. Perrin, O. M. Musa and J. W. Steed, *Chem. Soc. Rev.*, 2013, **42**, 1996-2015.
47. H. Ohno, T. A. Strobel, S. F. Dec, J. E. D. Sloan and C. A. Koh, *J. Phys. Chem. A*, 2009, **113**, 1711-1716.
48. J. J. Rivera and K. C. Janda, *J. Phys. Chem. C*, 2012, **116**, 19062-19072.
49. X. Cao, Y. Huang, W. Li, Z. Zheng, X. Jiang, Y. Su, J. Zhao and C. Liu, *Phys. Chem. Chem. Phys.*, 2016, **18**, 3272-3279.
50. A. Falenty, T. C. Hansen and W. F. Kuhs, *Nature*, 2014, **516**, 231-233.
51. C. Zhu, Y. Gao, W. Zhu, Y. Liu, J. S. Francisco and X. C. Zeng, *J. Phys. Chem. Lett.*, 2020, **11**, 7449-7461.
52. Y. Huang, C. Zhu, L. Wang, X. Cao, Y. Su, X. Jiang, S. Meng, J. Zhao and X. C. Zeng, *Sci. Adv.*, 2016, **2**, e1501010.
53. Y. Huang, C. Zhu, L. Wang, J. Zhao and X. C. Zeng, *Chem. Phys. Lett.*, 2017, **671**, 186-191.
54. Y. Liu, Y. Huang, C. Zhu, H. Li, J. Zhao, L. Wang, L. Ojamäe, J. S. Francisco and X. C. Zeng, *Proc. Natl. Acad. Sci. U.S.A.*, 2019, **116**, 12684.
55. M. D. Max, *Natural Gas Hydrate - In Oceanic and Permafrost Environments*, Kluwer Academic Publishers, Dordrecht, Netherlands, 2003.
56. J. Yang, A. Hassanpouryouzband, B. Tohidi, E. Chuvilin, B. Bukhanov, V. Istomin and A. Cheremisin, *J. Geophys. Res.*, 2019, **124**, 2551-2563.
57. N. Shakhova, I. Semiletov and G. Panteleev, *Geophys. Res. Lett.*, 2005, **32**, L09601.
58. E. Rivkina, V. Shcherbakova, K. Laurinavichius, L. Petrovskaya, K. Krivushin, G. Kraev, S. Pecheritsina and D. Gilichinsky, *FEMS Microbiol. Ecol.*, 2007, **61**, 1-15.
59. B. A. Buffett and O. Y. Zatsepina, *Mar. Geol.*, 2000, **164**, 69-77.
60. S. Faramawy, T. Zaki and A. A. E. Sakr, *J. Nat. Gas Sci. Eng.*, 2016, **34**, 34-54.
61. X. Ren, Z. Guo, F. Ning and S. Ma, *Earth-Sci. Rev.*, 2020, **202**, 103100.
62. P. Babu, A. Nambiar, T. He, I. A. Karimi, J. D. Lee, P. Englezos and P. Linga, *ACS Sustain. Chem. Eng.*, 2018, **6**, 8093-8107.
63. J. Zheng, F. Cheng, Y. Li, X. Lü and M. Yang, *Chin. J. Chem. Eng.*, 2019, **27**, 2037-2043.
64. Y.-N. Lv, S.-S. Wang, C.-Y. Sun, J. Gong and G.-J. Chen, *Desalination*, 2017, **413**, 217-222.
65. P. Sahu, S. Krishnaswamy, K. Ponnani and N. K. Pande, *Desalination*, 2018, **436**, 144-151.
66. Y. T. Ngan and P. Englezos, *Ind. Eng. Chem. Res.*, 1996, **35**, 1894-1900.
67. H. Xu, M. N. Khan, C. J. Peters, E. D. Sloan and C. A. Koh, *J. Chem. Eng. Data*, 2018, **63**, 1081-1087.
68. P. T. Ngema, C. Petticrew, P. Naidoo, A. H. Mohammadi and D. Ramjugernath, *J. Chem. Eng. Data*, 2014, **59**, 466-475.
69. M. Karamoddin and F. Varaminian, *Desalin. Water Treat.*, 2014, **52**, 2450-2456.
70. Y. Seo, D. Moon, C. Lee, J.-W. Park, B.-S. Kim, G.-W. Lee, P. Dotel, J.-W. Lee, M. Cha and J.-H. Yoon, *Environ. Sci. Technol.*, 2015, **49**, 6045-6050.
71. J.-H. Cha and Y. Seol, *ACS Sustain. Chem. Eng.*, 2013, **1**, 1218-1224.
72. Q. Lv, L. Li, X. Li and Z. Chen, *Energy Fuels*, 2015, **29**, 6104-6110.
73. Q. Lv, X. Li and G. Li, *Energy Procedia*, 2019, **158**, 5144-5148.
74. W. Choi, Y. Lee, J. Mok, S. Lee, J. D. Lee and Y. Seo, *Chem. Eng. J.*, 2019, **358**, 598-605.
75. S. D. Seo, S. Y. Hong, A. K. Sum, K.-H. Lee, J. D. Lee and B. R. Lee, *Chem. Eng. J.*, 2019, **370**, 980-987.
76. O. Y. Zatsepina and B. A. Buffett, *Fluid Ph. Equilibria*, 2002, **200**, 263-275.
77. P. S. R. Prasad, Y. Sowjanya and V. Dhanunjana Chari, *J. Phys. Chem. C*, 2014, **118**, 7759-7764.
78. P. Linga, C. Haligva, S. C. Nam, J. A. Ripmeester and P. Englezos, *Energy Fuels*, 2009, **23**, 5496-5507.
79. J.-n. Zheng, M.-j. Yang, Y. Liu, D.-y. Wang and Y.-c. Song, *J. Chem. Thermodyn.*, 2017, **104**, 9-15.
80. P. S. R. Prasad, B. S. Kiran and K. Sowjanya, *RSC Adv.*, 2020, **10**, 17795-17804.
81. O. Byl, J.-C. Liu, Y. Wang, W.-L. Yim, J. K. Johnson and J. T. Yates, *J. Am. Chem. Soc.*, 2006, **128**, 12090-12097.
82. A. I. Kolesnikov, J. M. Zanotti, C. K. Loong, P. Thiyagarajan, A. P. Moravsky, R. O. Loutfy and C. J. Burnham, *Phys. Rev. Lett.*, 2004, **93**, 035503.
83. K. V. Kumar, K. Preuss, M.-M. Titirici and F. Rodríguez-Reinoso, *Chem. Rev.*, 2017, **117**, 1796-1825.
84. P. Linga and M. A. Clarke, *Energy Fuels*, 2017, **31**, 1-13.
85. Y.-T. Seo, I. L. Moudrakovski, J. A. Ripmeester, J.-W. Lee and H. Lee, *Environ. Sci. Technol.*, 2005, **39**, 2315-2319.
86. Y. P. Handa and D. Y. Stupin, *J. Phys. Chem.*, 1992, **96**, 8599-8603.
87. Y. Zhang, X. Li, Z. Chen, Z. Xia, Y. Wang and G. Li, *Energy Procedia*, 2017, **142**, 4044-4049.
88. D. H. Smith, J. W. Wilder and K. Seshadri, *AIChE J.*, 2002, **48**, 393-400.

89. T. Uchida, T. Ebinuma and T. Ishizaki, *J. Phys. Chem. B*, 1999, **103**, 3659-3662.
90. T. Uchida, S. Takeya, E. M. Chuvilin, R. Ohmura, J. Nagao, V. S. Yakushev, V. A. Istomin, H. Minagawa, T. Ebinuma and H. Narita, *J. Geophys. Res.*, 2004, **109**.
91. P. Ilani-Kashkouli, H. Hashemi, F. Gharagheizi, S. Babaee, A. H. Mohammadi and D. Ramjugernath, *Fluid Ph. Equilibria*, 2013, **360**, 161-168.
92. K. Watanabe, K. Yokokawa and Y. Muto, presented in part at the 13th International Conference on Cold Regions Engineering, Orono, ME, USA, July, 2006.
93. D. Kim, D. W. Kim, H.-K. Lim, J. Jeon, H. Kim, H.-T. Jung and H. Lee, *Phys. Chem. Chem. Phys.*, 2014, **16**, 22717-22722.
94. Z. R. Chong, A. H. M. Chan, P. Babu, M. Yang and P. Linga, *J. Nat. Gas Sci. Eng.*, 2015, **27**, 178-189.
95. Y. Jin, Y. Konno and J. Nagao, *Energy Fuels*, 2012, **26**, 2242-2247.
96. S. Dai, J. C. Santamarina, W. F. Waite and T. J. Kneafsey, *J. Geophys. Res.*, 2012, **117**.
97. D. Kim and H. Lee, *Korean J. Chem. Eng.*, 2016, **33**, 1977-1988.
98. G. Bhattacharjee, A. Kumar, T. Sakpal and R. Kumar, *ACS Sustain. Chem. Eng.*, 2015, **3**, 1205-1214.
99. K. You, P. B. Flemings, A. Malinverno, T. S. Collett and K. Darnell, *Rev. Geophys.*, 2019, **57**, 1146-1196.
100. Y. Liang, Y. Tan, Y. Luo, Y. Zhang and B. Li, *J. Clean. Prod.*, 2020, **261**, 121061.
101. Y. Xie, R. Li, X.-H. Wang, T. Zheng, J.-L. Cui, Q. Yuan, H.-B. Qin, C.-Y. Sun and G.-J. Chen, *J. Nat. Gas Sci. Eng.*, 2020, **83**, 103520.
102. L. Borchardt, M. E. Casco and J. Silvestre-Albero, *ChemPhysChem*, 2018, **19**, 1298-1314.
103. S.-H. Yeon, J. Seol, D.-Y. Koh, Y.-j. Seo, K.-P. Park, D.-G. Huh, J. Lee and H. Lee, *Energy Environ. Sci.*, 2011, **4**, 421-424.
104. M. Khurana, Z. Yin and P. Linga, *ACS Sustain. Chem. Eng.*, 2017, **5**, 11176-11203.
105. D. Bai, G. Chen, X. Zhang and W. Wang, *Langmuir*, 2011, **27**, 5961-5967.
106. S. Alavi, K. Udachin and J. A. Ripmeester, *Chem. Eur. J.*, 2010, **16**, 1017-1025.
107. C. S. Kumar, *Microfluidic Devices in Nanotechnology: Fundamental Concepts*, John Wiley & Sons, Hoboken, NJ, USA, 2010.
108. L. Bocquet and E. Charlaix, *Chem. Soc. Rev.*, 2010, **39**, 1073-1095.
109. F. Ming and D.-q. Li, *Math. Probl. Eng.*, 2015, **2015**, 198986.
110. S. Taber, *J. Geol.*, 1930, **38**, 303-317.
111. L. Eickhoff, K. Dreischmeier, A. Zipori, V. Sirovinskaya, C. Adar, N. Reicher, I. Braslavsky, Y. Rudich and T. Koop, *J. Phys. Chem. Lett.*, 2019, **10**, 966-972.
112. H. Nada and Y. Furukawa, *Polym. J.*, 2012, **44**, 690-698.
113. A. Kaeck and U. Ziegler, in *Electron Microscopy*, ed. J. Kuo, Humana Press, Totowa, NJ, USA, 2014, vol. 1117, pp. 151-171.
114. D. Studer, W. Graber, A. Al-Amoudi and P. Egli, *J. Microsc.*, 2001, **203**, 285-294.
115. S. Bilgen and İ. Sarıkaya, *J. Nat. Gas Sci. Eng.*, 2016, **35**, 637-645.
116. Q. Wang and R. Li, *Renew. Sustain. Energy Rev.*, 2017, **74**, 715-720.
117. M. S. Gudipati and J. Castillo-Rogez, *The Science of Solar System Ices*, Springer Science & Business Media, New York, USA, 2012.
118. J. Klinger, D. Benest, A. Dollfus and R. Smoluchowski, *Ices in the Solar System*, D. Reidel Publishing Company, Dordrecht, Netherlands, 1985.
119. S. A. Sandford, L. J. Allamandola and T. R. Geballe, *Science*, 1993, **262**, 400.
120. H. Marsh and F. R. Reinoso, *Activated Carbon*, Elsevier Science & Technology Books, San Diego, CA, USA, 2006.
121. C. Cuadrado-Collados, F. Fauth, I. Such-Basañez, M. Martínez-Escandell and J. Silvestre-Albero, *Micropor. Mesopor. Mat.*, 2018, **255**, 220-225.
122. D. Katsuki, R. Ohmura, T. Ebinuma and H. Narita, *Philos. Mag.*, 2007, **87**, 1057-1069.
123. G. C. Fitzgerald, M. J. Castaldi and J. M. Schicks, *Ind. Eng. Chem. Res.*, 2014, **53**, 6840-6854.
124. S.-P. Kang, J.-W. Lee and H.-J. Ryu, *Fluid Ph. Equilibria*, 2008, **274**, 68-72.
125. L. Borchardt, W. Nickel, M. Casco, I. Senkovska, V. Bon, D. Wallacher, N. Grimm, S. Krause and J. Silvestre-Albero, *Phys. Chem. Chem. Phys.*, 2016, **18**, 20607-20614.
126. M. E. Casco, J. Silvestre-Albero, A. J. Ramírez-Cuesta, F. Rey, J. L. Jordá, A. Bansode, A. Urakawa, I. Peral, M. Martínez-Escandell, K. Kaneko and F. Rodríguez-Reinoso, *Nat. Commun.*, 2015, **6**, 6432.
127. J. Miyawaki, T. Kanda, T. Suzuki, T. Okui, Y. Maeda and K. Kaneko, *J. Phys. Chem. B*, 1998, **102**, 2187-2192.
128. A. Celzard and J. F. Maréché, *Fuel*, 2006, **85**, 957-966.
129. L. Yan, G. Chen, W. Pang and J. Liu, *J. Phys. Chem. B*, 2005, **109**, 6025-6030.
130. A. Siangsai, P. Rangsunvigit, B. Kitiyanan, S. Kulprathipanja and P. Linga, *Chem. Eng. Sci.*, 2015, **126**, 383-389.
131. P. Babu, D. Yee, P. Linga, A. Palmer, B. C. Khoo, T. S. Tan and P. Rangsunvigit, *Energy Fuels*, 2013, **27**, 3364-3372.
132. J.-W. Jung and J. C. Santamarina, *J. Cryst. Growth*, 2012, **345**, 61-68.
133. N. N. Nguyen, M. Galib and A. V. Nguyen, *Energy Fuels*, 2020, **34**, 6751-6760.
134. P. Skovborg and P. Rasmussen, *Chem. Eng. Sci.*, 1994, **49**, 1131-1143.
135. S. B. Cha, H. Ouar, T. R. Wildeman and E. D. Sloan, *J. Phys. Chem.*, 1988, **92**, 6492-6494.
136. P. Englezos, N. Kalogerakis, P. D. Dholabhai and P. R. Bishnoi, *Chem. Eng. Sci.*, 1987, **42**, 2647-2658.
137. W. N. R. W. Isahak, M. W. M. Hisham and M. A. Yarmo, *J. Chem.*, 2013, **2013**, 620346.
138. C. Cuadrado-Collados, J. Farrando-Pérez, M. Martínez-Escandell, L. A. Ramírez-Montoya, J. A. Menéndez, A. Arenillas, M. A. Montes-Morán and J. Silvestre-Albero, *Chem. Eng. J.*, 2020, **402**, 126276.
139. M. E. Casco, C. Cuadrado-Collados, M. Martínez-Escandell, F. Rodríguez-Reinoso and J. Silvestre-Albero, *Carbon*, 2017, **123**, 299-301.
140. H. Li, M. Eddaoudi, M. O'Keeffe and O. M. Yaghi, *Nature*, 1999, **402**, 276-279.
141. O. M. Yaghi, M. O'Keeffe, N. W. Ockwig, H. K. Chae, M. Eddaoudi and J. Kim, *Nature*, 2003, **423**, 705-714.
142. M. Eddaoudi, D. B. Moler, H. Li, B. Chen, T. M. Reineke, M. O'Keeffe and O. M. Yaghi, *Acc. Chem. Res.*, 2001, **34**, 319-330.

143. S. R. Batten, N. R. Champness, X.-M. Chen, J. Garcia-Martinez, S. Kitagawa, L. Öhrström, M. O'Keeffe, M. Paik Suh and J. Reedijk, *Pure Appl. Chem.*, 2013, **85**, 1715-1724.
144. X. Zhang, Z. Chen, X. Liu, S. L. Hanna, X. Wang, R. Taheri-Ledari, A. Maleki, P. Li and O. K. Farha, *Chem. Soc. Rev.*, 2020, **49**, 7406-7427.
145. Y. Lin, C. Kong, Q. Zhang and L. Chen, *Adv. Energy Mater.*, 2017, **7**, 1601296.
146. T. Asefa, K. Koh and C. W. Yoon, *Adv. Energy Mater.*, 2019, **9**, 1901158.
147. D. Kim, H.-K. Lim, H. Ro, H. Kim and H. Lee, *Chem. Eur. J.*, 2015, **21**, 1125-1129.
148. E. Soubeyrand-Lenoir, C. Vagner, J. W. Yoon, P. Bazin, F. Ragon, Y. K. Hwang, C. Serre, J.-S. Chang and P. L. Llewellyn, *J. Am. Chem. Soc.*, 2012, **134**, 10174-10181.
149. A. Ö. Yazaydin, A. I. Benin, S. A. Faheem, P. Jakubczak, J. J. Low, R. R. Willis and R. Q. Snurr, *Chem. Mater.*, 2009, **21**, 1425-1430.
150. J. Liu, Y. Wang, A. I. Benin, P. Jakubczak, R. R. Willis and M. D. LeVan, *Langmuir*, 2010, **26**, 14301-14307.
151. D. Kim and H. Lee, *RSC Adv.*, 2015, **5**, 2749-2755.
152. M. De Toni, R. Jonchiere, P. Pullumbi, F.-X. Coudert and A. H. Fuchs, *ChemPhysChem*, 2012, **13**, 3497-3503.
153. D. Kim, Y.-H. Ahn and H. Lee, *J. Chem. Eng. Data*, 2015, **60**, 2178-2185.
154. C. Serre, S. Bourrelly, A. Vimont, N. A. Ramsahye, G. Maurin, P. L. Llewellyn, M. Daturi, Y. Filinchuk, O. Leynaud, P. Barnes and G. Férey, *Adv. Mater.*, 2007, **19**, 2246-2251.
155. L. Mu, B. Liu, H. Liu, Y. Yang, C. Sun and G. Chen, *J. Mater. Chem.*, 2012, **22**, 12246-12252.
156. M. E. Casco, F. Rey, J. L. Jordá, S. Rudić, F. Fauth, M. Martínez-Escandell, F. Rodríguez-Reinoso, E. V. Ramos-Fernández and J. Silvestre-Albero, *Chem. Sci.*, 2016, **7**, 3658-3666.
157. Z. He, K. Zhang and J. Jiang, *J. Phys. Chem. Lett.*, 2019, **10**, 7002-7008.
158. C. Cuadrado-Collados, G. Mouchaham, L. Daemen, Y. Cheng, A. Ramirez-Cuesta, H. Aggarwal, A. Missyul, M. Eddaoudi, Y. Belmabkhout and J. Silvestre-Albero, *J. Am. Chem. Soc.*, 2020, **142**, 13391-13397.
159. K. A. Cychosz and A. J. Matzger, *Langmuir*, 2010, **26**, 17198-17202.
160. Z. Hu, Y. Chen and J. Jiang, *J. Chem. Phys.*, 2011, **134**, 134705.
161. J. Pérez-Pellitero, H. Amrouche, F. R. Siperstein, G. Pirngruber, C. Nieto-Draghi, G. Chaplais, A. Simon-Masseron, D. Bazer-Bachi, D. Peralta and N. Bats, *Chem. Eur. J.*, 2010, **16**, 1560-1571.
162. A. García Márquez, A. Demessence, A. E. Platero-Prats, D. Heurtaux, P. Horcajada, C. Serre, J.-S. Chang, G. Férey, V. A. de la Peña-O'Shea, C. Boissière, D. Grosso and C. Sanchez, *Eur. J. Inorg. Chem.*, 2012, **2012**, 5165-5174.
163. C. O. Ania, E. García-Pérez, M. Haro, J. J. Gutiérrez-Sevillano, T. Valdés-Solís, J. B. Parra and S. Calero, *J. Phys. Chem. Lett.*, 2012, **3**, 1159-1164.
164. G. Férey, C. Mellot-Draznieks, C. Serre, F. Millange, J. Dutour, S. Surblé and I. Margiolaki, *Science*, 2005, **309**, 2040.
165. R. G. AbdulHalim, P. M. Bhatt, Y. Belmabkhout, A. Shkurenko, K. Adil, L. J. Barbour and M. Eddaoudi, *J. Am. Chem. Soc.*, 2017, **139**, 10715-10722.
166. S. M. Towsif Abtab, D. Alezi, P. M. Bhatt, A. Shkurenko, Y. Belmabkhout, H. Aggarwal, Ł. J. Weseliński, N. Alsadun, U. Samin, M. N. Hedhili and M. Eddaoudi, *Chem*, 2018, **4**, 94-105.
167. D. Ongari, P. G. Boyd, S. Barthel, M. Witman, M. Haranczyk and B. Smit, *Langmuir*, 2017, **33**, 14529-14538.
168. S. S. Y. Chui, S. M. F. Lo, J. P. H. Charmant, A. G. Orpen and I. D. Williams, *Science*, 1999, **283**, 1148.
169. J. Bai, J. S. Francisco and X. C. Zeng, *Proc. Natl. Acad. Sci. U.S.A.*, 2018, **115**, 10263.
170. A. J. Mannix, B. Kiraly, M. C. Hersam and N. P. Guisinger, *Nat. Rev. Chem.*, 2017, **1**, 0014.
171. K. Koga, X. C. Zeng and H. Tanaka, *Phys. Rev. Lett.*, 1997, **79**, 5262-5265.
172. J. Bai, C. A. Angell and X. C. Zeng, *Proc. Natl. Acad. Sci. U.S.A.*, 2010, **107**, 5718.
173. P. Kumar, S. V. Buldyrev, F. W. Starr, N. Giovambattista and H. E. Stanley, *Phys. Rev. E*, 2005, **72**, 051503.
174. J. C. Johnston, N. Kastelowitz and V. Molinero, *J. Chem. Phys.*, 2010, **133**, 154516.
175. J. Bai and X. C. Zeng, *Proc. Natl. Acad. Sci. U.S.A.*, 2012, **109**, 21240.
176. M. Jia, W.-h. Zhao and L.-f. Yuan, *Chin. J. Chem. Phys.*, 2014, **27**, 15-19.
177. N. Giovambattista, P. J. Rossky and P. G. Debenedetti, *Phys. Rev. Lett.*, 2009, **102**, 050603.
178. R. Ma, D. Cao, C. Zhu, Y. Tian, J. Peng, J. Guo, J. Chen, X.-Z. Li, J. S. Francisco, X. C. Zeng, L.-M. Xu, E.-G. Wang and Y. Jiang, *Nature*, 2020, **577**, 60-63.
179. G. A. Kimmel, J. Matthiesen, M. Baer, C. J. Mundy, N. G. Petrik, R. S. Smith, Z. Dohnálek and B. D. Kay, *J. Am. Chem. Soc.*, 2009, **131**, 12838-12844.
180. R. Miyamoto, R. T. Hamazawa, M. Hirotsu, T. Nishioka, I. Kinoshita and L. J. Wright, *ChemComm*, 2005, 4047-4049.
181. W. S. Furey, C. V. Krishnamohan Sharma and M. J. Zaworotko, *Supramol. Chem.*, 1996, **8**, 9-11.
182. Z. He, P. Linga and J. Jiang, *Langmuir*, 2017, **33**, 11956-11967.
183. W.-H. Zhao, L. Wang, J. Bai, L.-F. Yuan, J. Yang and X. C. Zeng, *Acc. Chem. Res.*, 2014, **47**, 2505-2513.
184. W.-H. Zhao, J. Bai, L. Wang, L.-F. Yuan, J. Yang, J. S. Francisco and X. C. Zeng, *J. Mater. Chem. A*, 2015, **3**, 5547-5555.
185. H. Zhong, L. Li, R. Ma, J. Zhong, Y. Yan, S. Li, J. Zhang and J. Liu, *Phys. Chem. Chem. Phys.*, 2020, **22**, 5774-5784.
186. T. A. Strobel, C. J. Taylor, K. C. Hester, S. F. Dec, C. A. Koh, K. T. Miller and E. D. Sloan, *J. Phys. Chem. B*, 2006, **110**, 17121-17125.
187. R. Anderson, A. Chapoy and B. Tohidi, *Langmuir*, 2007, **23**, 3440-3444.
188. T. Sugahara, J. C. Haag, P. S. R. Prasad, A. A. Warntjes, E. D. Sloan, A. K. Sum and C. A. Koh, *J. Am. Chem. Soc.*, 2009, **131**, 14616-14617.
189. Y. Nagai, H. Yoshioka, M. Ota, Y. Sato, H. Inomata, R. L. Smith Jr. and C. J. Peters, *AIChE J.*, 2008, **54**, 3007-3016.
190. K. Ogata, S. Hashimoto, T. Sugahara, M. Moritoki, H. Sato and K. Ohgaki, *Chem. Eng. Sci.*, 2008, **63**, 5714-5718.
191. A. Talyzin, *Int. J. Hydrog. Energy*, 2008, **33**, 111-115.
192. D. Saha and S. Deng, *Langmuir*, 2010, **26**, 8414-8418.
193. H. Yoshioka, M. Ota, Y. Sato, M. Watanabe, H. Inomata, R. L. Smith Jr. and C. J. Peters, *AIChE J.*, 2011, **57**, 265-272.

194. H. P. Veluswamy and P. Linga, *Int. J. Hydrog. Energy*, 2013, **38**, 4587-4596.
195. K. Koga and H. Tanaka, *J. Chem. Phys.*, 2005, **122**, 104711.
196. J. Hou, J. Liu, J. Xu, J. Zhong, Y. Yan and J. Zhang, *Chem. Phys. Lett.*, 2019, **725**, 38-44.
197. S. Iijima, *Nature*, 1991, **354**, 56.
198. Z. Lin, Z. Zeng, X. Gui, Z. Tang, M. Zou and A. Cao, *Adv. Energy Mater.*, 2016, **6**, 1600554.
199. V. Buch and J. P. Devlin, *Water in Confining Geometries*, Springer Science & Business Media, New York, USA, 1 edn., 2003.
200. J. Wang, Y. Zhu, J. Zhou and X.-H. Lu, *Phys. Chem. Chem. Phys.*, 2004, **6**, 829-835.
201. M. C. Gordillo and J. Martí, *Chem. Phys. Lett.*, 2000, **329**, 341-345.
202. J. Martí and M. C. Gordillo, *Chem. Phys. Lett.*, 2002, **354**, 227-232.
203. M. C. Gordillo and J. Martí, *Chem. Phys. Lett.*, 2001, **341**, 250-254.
204. J. Martí and M. C. Gordillo, *Phys. Rev. B*, 2001, **63**, 165430.
205. C. Dellago, M. M. Naor and G. Hummer, *Phys. Rev. Lett.*, 2003, **90**, 105902.
206. D. J. Mann and M. D. Halls, *Phys. Rev. Lett.*, 2003, **90**, 195503.
207. H. Tanaka and K. Koga, *J. Chem. Phys.*, 2005, **123**, 094706.
208. W. Zhao, L. Wang, J. Bai, J. S. Francisco and X. C. Zeng, *J. Am. Chem. Soc.*, 2014, **136**, 10661-10668.
209. W. Zhao, J. S. Francisco and X. C. Zeng, *J. Phys. Chem. Lett.*, 2016, **7**, 4911-4915.
210. W. Zhao, J. Bai, J. S. Francisco and X. C. Zeng, *J. Phys. Chem. C*, 2018, **122**, 7951-7958.
211. H. Akbarzadeh, M. Abbaspour, S. Salemi and A. Nazarian, *New J. Chem.*, 2018, **42**, 7083-7095.
212. J. Li, H. Lu and X. Zhou, *Nanoscale*, 2020, **12**, 12801-12808.
213. L. Zhou, Y. Sun, Z. Yang and Y. Zhou, *J. Colloid Interface Sci.*, 2005, **289**, 347-351.
214. J. L. Cox, *Natural Gas Hydrates: Properties, Occurrence and Recovery*, Butterworth, USA, 1983.
215. M. E. Casco, M. Martínez-Escandell, E. Gadea-Ramos, K. Kaneko, J. Silvestre-Albero and F. Rodríguez-Reinoso, *Chem. Mater.*, 2015, **27**, 959-964.
216. S. Wang, C. M. McGuirk, A. d'Aquino, J. A. Mason and C. A. Mirkin, *Adv. Mater.*, 2018, **30**, 1800202.
217. C.-C. Hou and Q. Xu, *Adv. Energy Mater.*, 2019, **9**, 1801307.
218. T. A. Shifa and A. Vomiero, *Adv. Energy Mater.*, 2019, **9**, 1902307.
219. G. Sneddon, A. Greenaway and H. H. P. Yiu, *Adv. Energy Mater.*, 2014, **4**, 1301873.
220. X. Zhang, H. Liu and L. Jiang, *Adv. Mater.*, 2019, **31**, 1804508.
221. S. Yamaguchi, K. Morimoto, J. Fukuda and H. Suzuki, *Biosens. Bioelectron.*, 2009, **24**, 2171-2176.
222. G. Kwon, A. K. Kota, Y. Li, A. Sohani, J. M. Mabry and A. Tuteja, *Adv. Mater.*, 2012, **24**, 3666-3671.
223. U.-C. Yi and C.-J. Kim, *J. Micromech. Microeng.*, 2006, **16**, 2053-2059.
224. J.-h. Chang, D. Y. Choi, S. Han and J. J. Pak, *Microfluid. Nanofluid.*, 2010, **8**, 269-273.
225. S. Kuiper and B. H. W. Hendriks, *Appl. Phys. Lett.*, 2004, **85**, 1128-1130.
226. J. Heikenfeld, K. Zhou, E. Kreit, B. Raj, S. Yang, B. Sun, A. Milarcik, L. Clapp and R. Schwartz, *Nat. Photonics*, 2009, **3**, 292-296.
227. A. G. Papathanasiou, *Curr. Opin. Colloid Interface Sci.*, 2018, **36**, 70-77.
228. S. Kim, A. A. Polycarpou and H. Liang, *Appl. Surf. Sci.*, 2015, **351**, 460-465.
229. Y. Liu, Y. Gao and X. C. Zeng, *Nanoscale Horiz.*, 2020, **5**, 514-522.
230. D. Bratko, C. D. Daub, K. Leung and A. Luzar, *J. Am. Chem. Soc.*, 2007, **129**, 2504-2510.
231. C. D. Daub, D. Bratko, K. Leung and A. Luzar, *J. Phys. Chem. C*, 2007, **111**, 505-509.
232. J. L. Trick, C. Song, E. J. Wallace and M. S. P. Sansom, *ACS Nano*, 2017, **11**, 1840-1847.
233. G. Klesse, S. J. Tucker and M. S. P. Sansom, *ACS Nano*, 2020, **14**, 10480-10491.
234. T. Haynes, I. P. S. Smith, E. J. Wallace, J. L. Trick, M. S. P. Sansom and S. Khalid, *ACS Nano*, 2018, **12**, 8208-8213.
235. C. I. Lynch, S. Rao and M. S. P. Sansom, *Chem. Rev.*, 2020, **120**, 10298-10335.
236. X. Zhang, B. Wang, A. Alsalmeh, S. Xiang, Z. Zhang and B. Chen, *Coord. Chem. Rev.*, 2020, **423**, 213507.
237. S. Yuan, L. Feng, K. Wang, J. Pang, M. Bosch, C. Lollar, Y. Sun, J. Qin, X. Yang, P. Zhang, Q. Wang, L. Zou, Y. Zhang, L. Zhang, Y. Fang, J. Li and H.-C. Zhou, *Adv. Mater.*, 2018, **30**, 1704303.
238. K. Jayaramulu, F. Geyer, A. Schneemann, Š. Kment, M. Otyepka, R. Zboril, D. Vollmer and R. A. Fischer, *Adv. Mater.*, 2019, **31**, 1900820.
239. L.-H. Xie, M.-M. Xu, X.-M. Liu, M.-J. Zhao and J.-R. Li, *Adv. Sci.*, 2020, **7**, 1901758.
240. X. Liu, X. Wang and F. Kapteijn, *Chem. Rev.*, 2020, **120**, 8303-8377.
241. W. Xu and O. M. Yaghi, *ACS Cent. Sci.*, 2020, **6**, 1348-1354.
242. N. Hanikel, M. S. Prévot and O. M. Yaghi, *Nat. Nanotechnol.*, 2020, **15**, 348-355.
243. Z. Lei, Y. Xue, W. Chen, W. Qiu, Y. Zhang, S. Horike and L. Tang, *Adv. Energy Mater.*, 2018, **8**, 1801587.
244. C. S. Diercks and O. M. Yaghi, *Science*, 2017, **355**, eaal1585.
245. X. Lang, S. Fan and Y. Wang, *J. Nat. Gas Chem.*, 2010, **19**, 203-209.
246. Y. Song, Q. Sun, B. Aguila and S. Ma, *Adv. Sci.*, 2019, **6**, 1801410.
247. X. Ma and T. F. Scott, *Commun. Chem.*, 2018, **1**, 98.
248. B. O. Carter, W. Wang, D. J. Adams and A. I. Cooper, *Langmuir*, 2010, **26**, 3186-3193.
249. A. Ding, L. Yang, S. Fan and X. Lou, *Chem. Eng. Sci.*, 2013, **96**, 124-130.
250. L. Yang, S. Fan, Y. Wang, X. Lang and D. Xie, *Ind. Eng. Chem. Res.*, 2011, **50**, 11563-11569.
251. M. S. Silverstein and N. R. Cameron, in *Encyclopedia of Polymer Science and Technology*, John Wiley & Sons, Hoboken, NJ, 2002.
252. J. Duan, W. Jin and S. Kitagawa, *Coord. Chem. Rev.*, 2017, **332**, 48-74.
253. S. D. Kimmins and N. R. Cameron, *Adv. Funct. Mater.*, 2011, **21**, 211-225.
254. J. Gallagher, *Nat. Energy*, 2018, **3**, 86-86.
255. Y. Peng, V. Krungleviciute, I. Eryazici, J. T. Hupp, O. K. Farha and T. Yildirim, *J. Am. Chem. Soc.*, 2013, **135**, 11887-11894.

ARTICLE

Journal Name

256. S. Ma, D. Sun, M. Ambrogio, J. A. Fillinger, S. Parkin and H.-C. Zhou, *J. Am. Chem. Soc.*, 2007, **129**, 1858-1859.
257. S. M. Ghodsi, S. Anand, R. Shahbazian-Yassar, T. Shokuhfar and C. M. Megaridis, *ACS Nano*, 2019, **13**, 4677-4685.
258. P. F. Bernath, *Phys. Chem. Chem. Phys.*, 2002, **4**, 1501-1509.
259. D. Broseta, L. Ruffine and A. Desmedt, *Gas Hydrates 1: Fundamentals, Characterization and Modeling*, Wiley, Hoboken, NJ, USA, 2017.
260. S. Ho-Van, B. Bouillot, J. Douzet, S. M. Babakhani and J. M. Herri, *J. Environ. Chem. Eng.*, 2019, **7**, 103359.
261. M. Sarshar and A. H. Sharafi, *Desalin. Water Treat.*, 2011, **28**, 59-64.
262. M. Yang, J. Zheng, W. Liu, Y. Liu and Y. Song, *Energy*, 2015, **93**, 1971-1979.
263. J. Lee, K.-S. Kim and Y. Seo, *Chem. Eng. J.*, 2019, **375**, 121974.
264. S. Hong, S. Moon, Y. Lee, S. Lee and Y. Park, *Chem. Eng. J.*, 2019, **363**, 99-106.
265. M. Yang, Y. Song, L. Jiang, W. Liu, B. Dou and W. Jing, *Appl. Energy*, 2014, **135**, 504-511.
266. Y.-A. Lim, P. Babu, R. Kumar and P. Linga, *Cryst. Growth Des.*, 2013, **13**, 2047-2059.
267. J. Zheng, B.-Y. Zhang, Q. Wu and P. Linga, *ACS Sustain. Chem. Eng.*, 2018, **6**, 11913-11921.
268. P. Linga, P. Babu and A. P. Nambiar, *Singapore Pat. PCT/SG2018/050083*, 2018.
269. R. Das, M. E. Ali, S. B. A. Hamid, S. Ramakrishna and Z. Z. Chowdhury, *Desalination*, 2014, **336**, 97-109.
270. K. Roy, A. Mukherjee, N. R. Maddela, S. Chakraborty, B. Shen, M. Li, D. Du, Y. Peng, F. Lu and L. C. García Cruzatty, *J. Environ. Chem. Eng.*, 2020, **8**, 103572.
271. M. Kadhom and B. Deng, *Appl. Mater. Today*, 2018, **11**, 219-230.
272. Z. Cao, V. Liu and A. Barati Farimani, *Nano Lett.*, 2019, **19**, 8638-8643.